Neil Sawhney
Candidate for BE of Mechanical Engineering,
Cooper Union for the Advancement of Science and Art,
email: Neil@Neil-Sawhney.com

Preston Xu
Candidate for BE of Mechanical Engineering,
Cooper Union for the Advancement of Science and Art,
email: Preston@prxu.dev

Jiah Jin
Candidate for BE of Mechanical Engineering,
Cooper Union for the Advancement of Science and Art,
email: zhihui0730@gmail.com

Design and Fabrication of a Compliant Solar Tracker

Solar tracking mechanisms have demonstrated the potential to greatly boost the efficiency of Solar Photovoltaic (PV) panels. However, issues such as high startup costs, maintenance needs, and complex designs hinder the widespread adoption of current available systems. We present a novel approach to solar tracker design by integrating compliant mechanisms to address these challenges, specifically aiming towards improving widespread adoption in suburban residential applications. The proposed design aims to reduce cost and complexity by eliminating traditionally-required moving parts. Through this approach, the cost, viability, and longevity of solar tracking mechanisms are greatly improved, which drives the initiative to sustainably support the power grid.

Keywords: Compliant Mechanism, Solar Tracking, Single-Axis, Design Optimization

1 Introduction

Solar trackers are devices designed to optimize the efficiency of solar panels by adjusting their orientation to face the sun continually. This movement ensures that the panels capture the maximum amount of solar energy throughout the day. Solar trackers are known to increase net energy output by up to 50% depending on their geographical region compared to an equivalently sized fixed-mounted panel[1].

Unfortunately, tracking systems aren't frequently used in the United States because of their large associated start-up costs, increased need for regular maintenance, and difficulty to scale. Currently, solar tracker use in the United States is highly concentrated on the West Coast, with 80 percent of utility-scale Photovoltaics (PV) units implementing some form of tracking compared to only 20 percent on the East Coast [1]. This is due to ideal weather conditions (higher light intensity, more sunny days) presenting a much higher value proposition for implementing utility scale solar instead of bearing the high cost and slow return of installing a residential-scale solar system.

We aim to take the existing concepts and methodology behind solar tracking and apply principles of compliant mechanisms to eliminate moving parts and reduce design and manufacturing complexity. Our solution will increase long-term maintainability while minimizing start-up costs, making small-scale solar systems a viable proposition even with non-ideal weather conditions.

2 Prior Art

2.1 Single Axis vs Dual Axis. Sun tracking systems can be classified into two types —single-axis and dual-axis —based on their degrees of freedom.

Single-axis trackers rotate mainly on an east-west axis, whereas dual-axis trackers add a north-south rotational capacity to the east-west movement as shown in Figure 1. Both single-axis and dual-axis tracking systems exhibit better performance over the fixed-tilt solar panel, shown in Table 1. Compared to the fixed-axis system, the single-axis improves the energy output by up to 40%, and the dual-axis improves the energy output by up to 50%[2].

However, this boost in energy generation comes with increased complexity and higher initial costs. Consequently, the economic feasibility and payback period extend accordingly, as it takes longer for the energy savings to offset the initial investment and continuous maintenance costs for more complex tracking systems.

Geographic latitude plays a crucial role in the effectiveness of these systems. In regions like Arizona, where there is minimal north-south seasonal variation in solar angle, the advantage of a dual-axis tracker is less pronounced. Here, investing in additional panels to capitalize on peak sunlight hours might yield a better return. On the contrary, in places with significant seasonal sunlight shifts such as Alaska, a dual-axis tracker can be substantially more advantageous. The wide variation in peak sunlight hours throughout the year makes the dual-axis system's ability to follow the sun's position a valuable feature for maximizing energy capture[3].

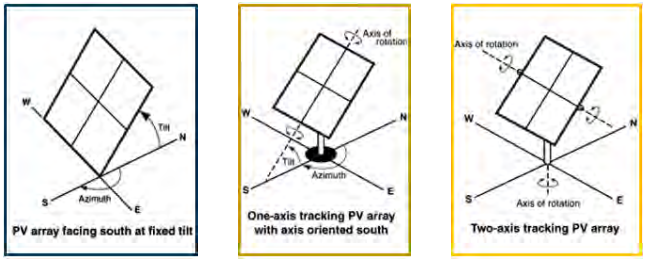

(*a*) Fixed Tilt (*b*) Single Axis (*c*) Dual Axis

Fig. 1 Comparison of solar tracker types [1]

Table 1 Cost Comparison Table [4]

Tracking Type	Power Output Gain %	Total Cost / 1 KW Panel [$/KW]	Payback Period [yr] [5]
Fixed-Tilt	0%	190-670	17.1
Single-Axis	20-40%	205-840	13.4
Dual-Axis	40-50%	600-1,900	11.6

2.2 Compliant Mechanisms. A compliant mechanism achieves motion via the deformation of flexible components. Unlike traditional rigid-body joints, compliant mechanisms usually need fewer moving parts, suffer less friction wear, and have more predictable failure modes. Their use can often greatly reduce the manufacturing cost of mechanisms that require repetitive motion.

2.3 Injection Molded Living Hinge. One example of a compliant mechanism used in the plastic manufacturing industry is the

February 18, 2025

[1] Areas closer to the equator will benefit less because the sun is more frequently overhead, while places further from the equator experience greater incidence angles.

living hinge, shown in Figure 2. Compliant mechanisms such as the living hinge reduce assembly and production costs. While most conventional hinges require some type of pin like a screw or metal rod, a living hinge is a uni-body design. A properly designed and applied living hinge can also last well over a million cycles[6].

Fig. 2 Example of a living hinge in a ketchup bottle cap

2.4 Kirigami-Based Compliant Solar Tracker. One of the few documented designs for a compliance-based solar tracker is the Kirigami-inspired compliant dual-axis solar tracker. The design combines a compliant mechanism, influenced by kirigami art, with an integrated system of solar panels, sensors, and controls. This system operates passively, using the differential expansion of thin metal sheets to naturally tilt the structure towards the sun's heat [7].

However, some notable drawbacks include the complexity of manufacturing due to the intricate kirigami design and increased maintenance requirements due to the structure's sensitivity to environmental conditions such as wind and snow.

Comparatively, compliant flexure beams like those presented in [8] provide a simpler mechanical structure, while offering superior manufacturability and greatly reduced maintenance requirements due to a more robust structure.

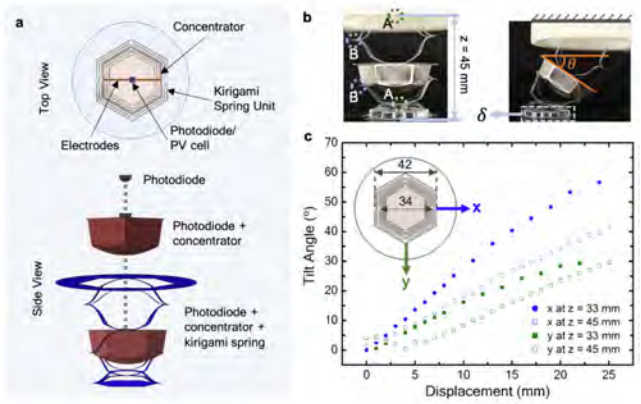

Fig. 3 Kirigami Inspired Passive Compliant Solar Tracker.

3 Requirements

3.1 Functional Requirements. This section outlines the functional requirements necessary for the development of an optimal solar tracking system. These requirements focus on ensuring that the system is cost-effective, performs efficiently, and operates reliably under various environmental conditions.

3.1.1 Cost Requirement. The proposed solar tracking system should be cost-effective, with startup and maintenance costs significantly lower than those of comparable existing solutions. Existing solutions for a single axis rooftop tracker typically costs 5 to 15 times the cost of the panels they mount [9]. Therefore, a cost equal to or lower than 5 times the cost of the mounted panel would be a reasonable goal to decrease the initial startup costs associated with solar tracking.

The system's design and implementation should focus on utilizing cost-effective materials and technologies, without compromising performance and durability. Moreover, the maintenance costs should also be minimized. This can be achieved by designing a system with fewer moving parts that are less susceptible to wear and tear, thus reducing the frequency of repairs and replacements. Existing solutions for single axis rooftop trackers require maintenance around twice a year. This maintenance generally involves lubricating components such as bearings and gears and inspecting motors to ensure they are functioning properly[9]. Therefore, a reasonable requirement would be to achieve a maintenance free life span of longer than half a year.

3.1.2 Performance Requirement. The proposed solar tracking system should demonstrate comparable performance in terms of both efficiency and reliability. The goal is to achieve a 30% increase in net energy output compared to a fixed-tilt system. This performance target is based on industry-standard benchmarks used to evaluate solar tracker performance, as outlined in [10].

Reliability is a critical aspect of performance. The system should sustain its performance over time, even under environmental stressors such as wind loads, temperature fluctuations, and salt corrosion, common in coastal areas. With these in mind, the proposed system must still be able to meet a product lifespan of 10-20 years, the average for tracking systems mentioned in [10].

Furthermore, the system should offer seamless operation, with minimal downtime or need for manual intervention. In the event of a system error or failure, the design should facilitate easy troubleshooting and restoration of normal operation.

3.2 Codes and Regulations. To ensure that our solar tracking system meets precise standards, all technical drawings shown in Appendices A - F follow the American Society of Mechanical Engineers (ASME) standard for Dimensioning and Tolerancing. This standard provides guidelines and definitions for standard practices used in engineering drawings. Section 1 enforces the importance of uniform dimensioning which promotes clarity and minimizes ambiguities, ensuring components fit accurately during assembly. Additionally, because our solar tracker is intended to operate on rooftops, we comply with weight requirements governed by the International Building Code (IBC)[11]. The IBC mandates that the weight of any rooftop-mounted equipment must not exceed 4,000 pounds per 100 square feet of roof area. Our design adheres to this regulation, ensuring that the solar tracker is safe for installation on residential rooftops. Through the use of environmentally safe materials, we follow the ISO 14001 standard for an effective environmental management system (EMS)[12], ensuring our operations are environmentally responsible. Lastly, for all performance testing, we comply with the IEC 61724-1 standard[13], which provides procedures for measuring and analyzing the performance of photovoltaic systems.

4 Design and Manufacturing

In the case of solar trackers, the benefits of implementing a compliant mechanism are potentially even greater than that of the living hinge. Due to the structural requirements of a solar tracker, bearings and gears, or precision bushings are required. These experience frictional wear which necessitates frequent maintenance such as lubrication and replacement. Dirt, rust, and ice can seize nearly any frictional hinge. Implementing a compliant mechanism eliminates these issues.

4.1 Mechanical Design. This section aims to provide insight on the thought process behind the selection of materials and components as well as how we selected and implemented a compliant

mechanism into the design of our prototype solar tracker. In addition to meeting the functional and design requirements outlined in section 3, our driving design philosophy is to reduce the number of moving components while keeping a minimalistic, easily manufacturable design so that reliability and maintainability is improved while the cost of production is lowered.

Renders of our final design is shown in Figure 4, Figure 5, and Figure figure 6.

Fig. 4 Isometric Rendered View of the Final Design

(*a*) Assembled View

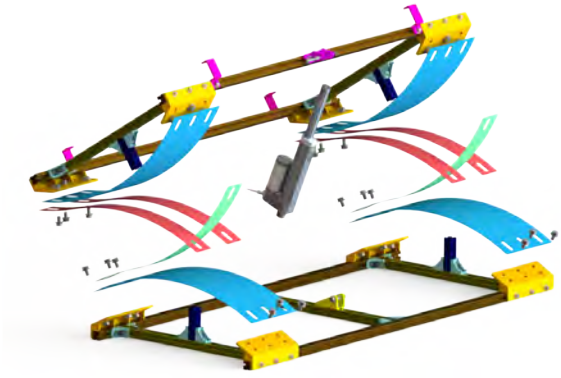

(*b*) Exploded View

Fig. 5 Colored Renders at Full Actuator Expansion: The contact rollers are colored light blue, the brackets are pink and yellow, and the flexures are green and red

4.1.1 Compliant Mechanism Selection. The application of a compliant, single-axis solar tracker necessitates the selection of a compliant system with one rotational degree of freedom. Many classes of compliant mechanisms satisfy this requirement, including all those shown in 7. However, we selected a compliant rolling joint to inform our design for the reason that it can be easily made from off-the-shelf parts, has a large range of motion, and is also fully constrained.

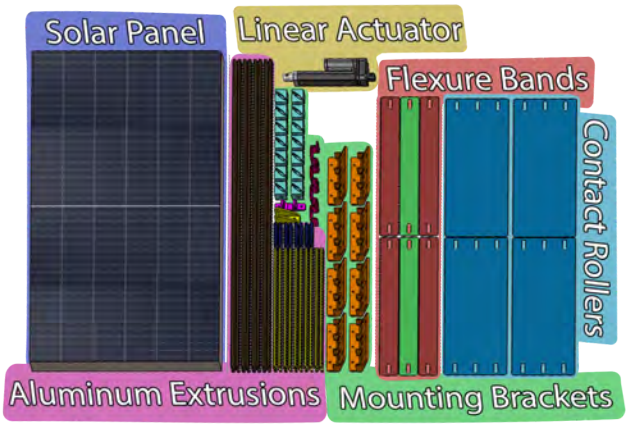

Fig. 6 All Components Layed Out and Labelled (hardware such as nuts and bolts are not shown)

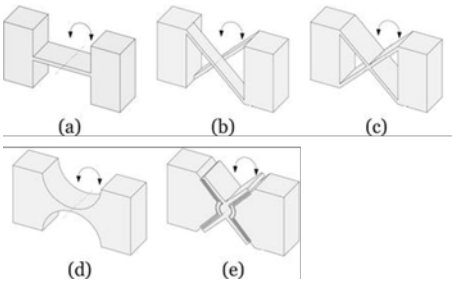

Fig. 7 Various Types of Compliant Flexure Hinges [14]

This mechanism is known as a compliant rolling-contact joint (CRJ) as shown in Figure 8. It consists of two rigid contact rollers on the top and bottom with compliant flexure bands of the same shape spanning between them. CRJ's rotate about a dynamic rotation axis going through the contact-point between the top and bottom rollers. This minimizes friction wear due to the ability to "roll without slipping". At any time, the structure is fully constrained other than its current rotational axis, meaning that it can achieve strength and stability equivalent to a conventional fixed-pivot design.

Our implementation of the CRJ is shown in Figure 9. The flexures and the contact rollers are designed to be punched out of 0.032" thick 6061 aluminum sheet metal. This keeps the cost of manufacturing low as well as the weight and packaging volume of the structure. The flexures on our prototype were laser cut because it is cheaper when making a singular unit, but the end product is nearly identical. The contact rollers are designed to have a radius of curvature of 430 mm, which would allow a maximum tilt angle of 60° in both compression and expansion. However, the heads of the bolts used to attach the flexures and contact rollers to the mounting bracket limit the maximum tilt angle. For this reason, the bolts are alternated on top and bottom which enables the tracker to achieve $\tilde{3}5°$ on each side.

4.1.2 Panel Selection. We have chosen a compact and lightweight 100W solar panel, ideal for areas where larger panels are not practical, such as residential homes and RV rooftops. These panels are smaller than the typical 66"x40" dimensions of 250-365W panels[16] and are designed to be more affordable by 10%. The dimensions of our selected panel is 40"x18"x1.4".

4.1.3 Material Selection. The material for our design was selected based on three main criteria: structural durability (yield, fatigue), weather resistance (rust, corrosion), and cost. The scope

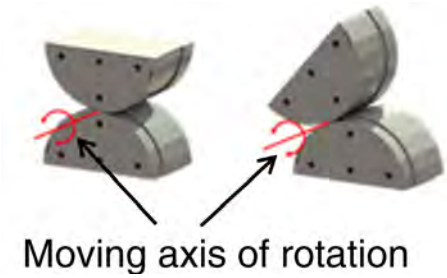

Fig. 8 Rolling Compliant CRJ[15]

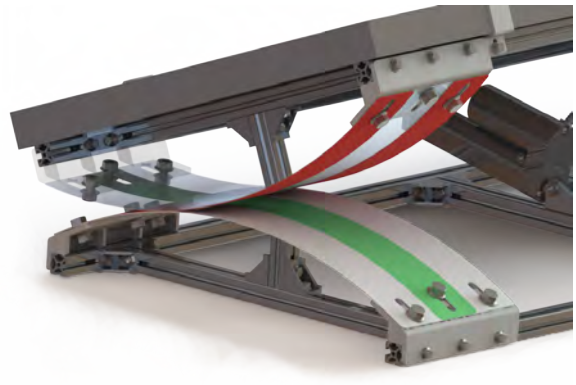

Fig. 9 Closeup Render of the CRJ: Flexures are colored red and green. The bolts which hold the flexures and contact rollers to the mounting bracket are alternated on top and bottom to allow a greater angle of tilt.

of our analysis was narrowed down to 6061 Aluminum and 1095 Steel, two widely used and readily available varieties of aluminum and steel with balanced mechanical properties. For FOS against yielding, we define an acceptable minimum yield FOS to be 1.5.

	1095 Steel	**6061 Aluminum**
Tensile Yield Strength (MPa)	570	276
Fatigue Stress at 10^6 Load Cycles (MPa)	200	100
Endurance Limit	Yes	No
Weather Resistance	Rust prone	Protective Corrosion
Cost / Material Area ($\$/in^2$)	.17	.07

Table 2 Comparison of 1095 Steel and 6061 Aluminum

Our analysis concluded that 1095 steel has a higher yield strength as well as a higher fatigue stress and a defined endurance limit. However, 6061 aluminum is more cost-efficient and more weather-resistant due to its ability to form a protective corrosion layer as opposed to rusting through the material like 1095 steel [17]. We define cost-efficiency as the cost required per area ($\$/in^2$) since our designed geometry dictates area while the material thickness is constrained by targeting equivalent plate stiffness ($E \cdot I$ remains constant so aluminum sheets are selected 1.5 times thicker than steel sheets). Additionally, the flexures for our design are not high stress components, whereas weather resistance is extremely important for longevity in an outdoor product. For these reasons, we selected 6061 aluminum as the material for the sheet metal components of our design.

The material thickness for our design was selected to maintain an assembly force within an "ergonomic" range while still maintaining structural integrity. As such, we defined the max assembly force to be below 50 Newtons while maintaining the minimum yield FOS to be 1.5.

	0.02"	0.025"	0.032"
Required Assembly Force (N)	12	23	46
Yield FOS	1.32	1.57	1.89

Table 3 Comparison of 6061 Aluminum Sheet Metal Thickness

Table 3 shows a few different material thicknesses we analyzed. Our design lends itself toward strength maximization as the criteria for the flexure bands and actuation force minimization as the criteria for the contact rollers. This means we aimed to select the thinnest material possible possible for the contact rollers and the thickest material possible for the flexure bands such that both selected materials still satisfy the 50 Newton actuation force and 1.5 yield FOS requirements. We found that 0.025", 6061 for the flexure straps and 0.032", 6061 for the contact roller best satisfied these constraints.

4.1.4 Frame. Our design uses 2020 aluminum extrusions for all framing components. While these are weather resistant and convenient during rapid prototyping, they are not cost effective. During mass production, these extrusions can be replaced with square cross section beams or even I beams. A list of all the extrusion sizes that make up our design is shown in Table 4. The small 70 mm extrusions which support the middle of each contact roller were added for rigidity. With minor adjustments these can potentially be removed in future versions of the design. This is discussed in more detail in Section 8.

Table 4 2020 Aluminum Extrusion Cut List

Length	Quantity
1000 mm	4
390 mm	5
70 mm	4

4.1.5 Actuation Selection. For our actuation mechanism, we selected a standard off-the-shelf linear actuator with a 150 mm stroke length, 410 mm extended length, and 260 mm retracted length. It offers a max load of 900N. A linear actuator was selected because it is reliable, cost effective, and can be easily swapped out without any special knowledge or equipment. It also features an internal worm gear mechanism that prevents the actuator from moving when not powered, which is essential for the efficiency of our design.

Due to the moving rotational axis, other actuation methods add complexity that makes installation more difficult and the need for maintenance more likely. Although using multiple linear actuators would be easier to design (since at least one actuator can always be acting in the most optimal pushing configuration), we opted for the use of just one carefully placed actuator to minimize cost, energy usage, and complexity.

When using a single linear actuator, it's critical to select the right size and position. If the actuator is attached to both the top and bottom portions of the panel on the same side as shown in Figure 10(*a*) and 10(*b*) the tracker would be unable to compress fully. Selecting a smaller actuator would not help, the shortest distance from the panel edge to the bottom frame edge at full compression is less than half the maximum distance at full expansion, and a

(*a*) Edge Placement - Fully Compressed

(*b*) Edge Placement - Fully Expanded

Fig. 10 Actuator Placement Examples

linear actuator can't extend more than double its contracted length. By sliding the bottom attachment towards the opposite end of the tracker as shown in Figure 12, it becomes possible to achieve a full range of motion. However, there are still constraints. Sliding the bottom connection too far to the opposite end of the middle extrusion can make it impossible for any linear actuator to achieve the full range of motion. This is once again because the shortest distance from the opposite diagonal extrusion at full compression is less than half the maximum distance at full expansion. This leaves a small window of acceptable positions which varies for each size actuator.

To find the most optimal position within this window, the torque must be considered. As shown in Figure 11, as the bottom attachment point is moved further away from the top attachment point, the angle between the force vector and moment arm decreases, reducing the efficiency of our design. Therefore, the most optimal sized actuator is the smallest which can still reach the top attachment point from the bottom attachment point. The most optimal location of the bottom attachment point is achieved by compressing the actuator as much as possible and fixing the bottom attachment point when the panel is tilted as much as possible. The actuator in its optimal position is shown in Figure 12.

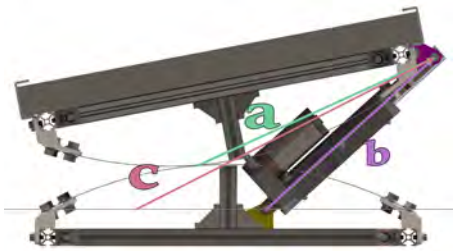

Fig. 11 Side view of the tracker which demonstrates how torque is optimized through the correct placement of the actuator. *a* represents the moment arm from the rotation axis to the top actuator attachment point. *b* and *c* represent the vector from the bottom attachment point to the top actuator attachment point for various size actuators.

Although custom sized actuators are available for purchase, they can be more than 5 times more expensive than off the shelf alternatives. For this reason, our selected actuator is chosen from a list of 6 standard sizes that are available at a competitive price by a variety of sellers. The actuator with 150 mm stroke length, 410 mm extended length, and 260 mm retracted length was the smallest from this list that still satisfied the constraints mentioned above.

4.1.6 Custom Brackets. Although all brackets are intended to be stamped out of sheet metal, we did not have access to the machinery required to achieve this. We also did not have access to a machine that can bend 3/16" aluminum sheet metal. For this reason, we opted to use 3D printed brackets for our prototype, While their shape was chosen to replicate the shape of the sheet metal

Fig. 12 Diagonal Placement - Fully Compressed

brackets as much as possible, minor changes had to be made to account for the lower strength of 3d printed components. For example, all the brackets were 8 mm thick, and the mounting bracket which holds the contact rollers included ribs which rest on the extrusion to prevent the bracket from bending under load. Lastly, the top actuator attachment bracket is bolted on the sides instead of in the middle for extra strength. If this design was to be mass-produced, the brackets would need very few changes. Technical drawings for the brackets are shown in Appendices A, F, D, and E.

4.1.7 Hardware. To make the assembly process as simple as possible, we selected a standard set of nuts and bolts. For attaching the flexures to the mounting brackets, M8 bolts were selected. For all other locations, M5 bolts were used. All bolts are flanged with hexagonal heads so that no washers are necessary and everything can be assembled with a single socket set. The quantities of all hardware components are shown in Table 5.

Table 5 Hardware List

Component	Quantity
M8 Bolts - 12 mm	24
M5 Bolts - 10 mm	76
M8 Nuts	24
M5 T-Nuts	76
2020 Corner Bracket	20

4.1.8 Packaging and Assembly. Because nearly the entire structure is made of flat sheet metal and straight extrusions, the packaging volume can be kept extremely small. A potential arrangement of the tracker components are shown in figure 13. This layout, which can be further optimized, allows all the components of the tracker to be packaged in a box that is just 3'x6"x2". This compact design reduces shipping cost and improves the ease of handling and assembly on-site, thereby enhancing the overall logistical efficiency and installation speed of the solar tracking system.

The assembly is straightforward and can be performed by a single person without any special training. The general process is outlined below:

- Loosely assemble both the top and bottom frame by using the corner brackets.
- Place the mounting brackets flush to the edge of the extrusions and align the middle extrusions with the center hole.
- Tighten all screws of the frame and mounting brackets.
- Loosely attach the contact rollers and center flexures to the bottom frame on one side.

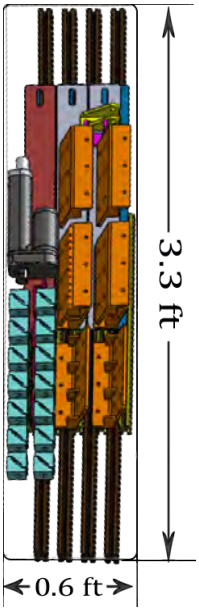

Fig. 13 Proposed Package Scheme

- Loosely attach the contact rollers and outer flexures to the top frame on one side.
- Place the top frame over the bottom frame and attach the remaining contact rollers and flexures.
- Tighten all the screws.
- Attach the top actuator bracket and loosely attach the bottom actuator bracket.
- Fix the actuator in its fully contracted position to the top and bottom brackets using the pin and safety pin.
- Tilt the actuator to its maximum angle at full compression and simultaneously tighten the bottom actuator bracket.
- Slide the panel into the top panel brackets and tighten all the screws.

4.1.9 Initial Prototype. The prototype came together nearly identically to the CAD assembly, the fully assembled prototype is shown in Figure 14 and 15. The structure is rigid and fully constrained. The structure can be reliably lifted from the top half of the mechanism without any noticeable gap emerging between the contact rollers. The most significant difference between the intended design and the physical prototype is the maximum compression and expansion angles. While the mechanism was designed to achieve a maximum compression and expansion angle of 40°, it is only capable of expansion and compression angles of 35.2° and 31.5° respectively. This is because the heads of the bolts were not considered when initially deciding on the radius of curvature to use for the contact rollers. Although this mistake was noticed in the CAD assembly before creating the prototype, the incorrect size of material was already ordered so we decided to continue with the semi-flawed design. Recommendations for rectifying this issue in future versions of the design are mentioned in Section 8.

Fig. 14 Final Assembled Prototype at Full Expansion

Fig. 15 Final Assembled Prototype CRJ Closeup View

4.2 Electrical and Software Design. The linear actuator is controlled by two relays, where each relay is in control of one direction of movement. These relays are switched by a Raspberry Pi Zero 2 W. Although the Raspberry Pi Zero 2W is inexpensive at $15, it is still an overkill solution chosen for prototyping convenience. The mass produced version can include any cheap microcontroller such as the ESP32-C3-WROOM-02 which can be purchased for under $0.50[18]. In addition, a single microcontroller could operate many panels simultaneously. This Raspberry Pi is configured to activate the relays according to the desired angle of the solar panel. The power source for the Raspberry Pi, linear actuator, and the relays is a 12V 2A power supply. The Raspberry Pi is connected to the power supply through a 5V linear regulator.

The Raspberry Pi has Wi-Fi connectivity, offering remote monitoring and control of the solar tracker. This connectivity also enables the tracker to periodically retrieve data about the solar position for any given day, eliminating the need for a sun sensor. The code for the Raspberry Pi is written in Python and is available in a Github Repository using the following link.

Notably, there is no encoder or sensor to provide feedback to the Raspberry Pi. Instead, the Raspberry Pi is programmed to actuate the linear actuator for a set amount of time to reach the desired angle. This method was chosen to reduce the complexity of the system and to minimize the cost. In order to create a mapping between the actuation time and the desired angle, a lookup table was created. This table was generated by actuating the linear ac-

tuator for a specific amount of time and measuring the resulting angle. The actuation time-tables for contraction and expansion are shown in Table 6. The expansion takes longer than the contraction because it requires more energy to expand. This is demonstrated in Section 6.3. For desired angles between those in the lookup table, the actuation time is calculated using a linear interpolation between the two nearest entries.

Because there is no feedback, frequent homing is essential. The linear actuator has built in logic that stops it from moving at its endpoints. Because the mechanism is designed to be at maximum angle when the actuator is fully expanded, extending the actuator to full expansion is equivalent to homing. Therefore, the tracker self homes at least once a day when the sun ducks under the horizon.

Before normal operation, several user-defined parameters must be set. These include the time interval between each actuation, the longitude and latitude of the tracker, the local timezone, the rooftop angle, and the heading of the tracker. The rooftop angle is the angle between the roof and the ground, and the heading is the angle between the tracker and true north.

At the start of each day, the Raspberry Pi retrieves the solar position data for that day using the pvlib [19] library. The optimal angle for the solar panel to maximize energy output is then computed for each time at the user-defined interval using a simple projection algorithm from [20]. The actuation time to get from each angle to the next is then calculated for each update interval by interpolating from the lookup table shown in Table 6. The Raspberry Pi then waits until the next update interval to actuate the linear actuator to the next angle.

5 Fatigue Analysis

In general, fatigue is a very important failure mode for compliant mechanisms. In our design, it is critical for the flexure bands to achieve a long fatigue life in order to fulfill the design goal of being low-cost and low-maintenance. In this section, we provide evidence to show why fatigue failure is a non-concern in our specific application. This hypothesis is experimentally validated in Section 6.2.

Fatigue analysis is most important in cases when the application necessitates a high amount of load cycles. These load cycles are commonly on the order of $10^4 - 10^8$ cycles. Since solar tracking by nature necessitates only 1 full stress cycle per day, the total number of stress load cycles undergone by the flexure bands throughout their entire lifetime will be relatively low. For context, 10 years, which is the average lifespan of the linear actuator, amounts to only 3650 stress cycles. To account for uncertainty, our own fatigue test in Section 6.2 runs through 50 years worth of stress cycles.

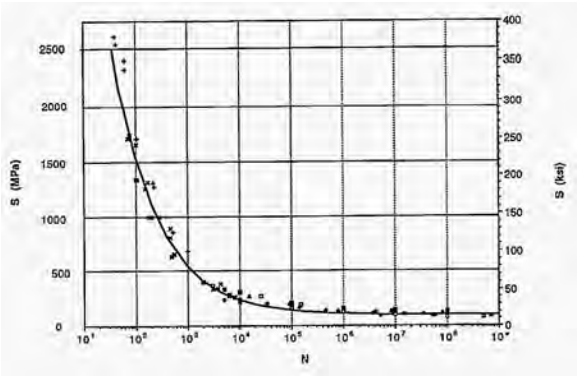

Fig. 16 S-N Curve Fit for 6061 Aluminum [21]

Figure 16 shows an S-N curve fit for 6061 aluminum. Given our max stress of $\sigma_{max} = \sigma_y/\text{Yield FOS} = 184\text{MPa}$, we can see that when subjected to a fully-reversed cyclic stress of this amplitude, 6061 aluminum has a fatigue life of around $5 \cdot 10^4$ cycles. This is equivalent to an operating lifetime of 139 years, which is well beyond even extreme estimates for the lifetime of other components on the tracker.

Actuation Time [ms]	Desired Angle [Deg]
0	-35.2
425	-33.7
850	-32.1
1275	-30.2
1700	-28.1
2125	-25.9
2550	-23.6
2975	-21.1
3400	-18.2
3825	-14.7
4250	-11.2
4675	-7.5
5100	-3.8
5525	0.6
5950	5
6375	9.5
6800	14
7225	19
7650	23.8
8075	27.5
8500	31.5

(*a*) Contraction Actuation Time-Table

Actuation Time [ms]	Desired Angle [Deg]
0	31.5
425	28.3
850	23.9
1275	19.4
1700	14.9
2125	10.1
2550	5.7
2975	1.4
3400	-2.6
3825	-6.8
4250	-10.5
4675	-13.8
5100	-17.1
5525	-20.2
5950	-22.9
6375	-25.0
6800	-27.5
7225	-29.6
7650	-31.3
8075	-33.3
8500	-34.6
9000	-35.2

(*b*) Expansion Actuation Time-Table

Table 6 Actuation Time-Tables for Contraction and Expansion

6 Testing

Due to our design utilizing actuation time instead of a closed loop control to reach a particular actuator length, it was essential to validate the tracker's ability to accurately and precisely reach a given angle. Section 6.1 outlines the relevant test procedure and findings for the consistency test. Since our system relies on compliant flexures, reduced efficiency due to the required energy input to bend the flexures was a concern. However, Section 6.3 demonstrates that this issue did not arise. Although the focus of this paper is on an application of compliant mechanisms, it is nonetheless important to characterize our system's overall performance as a functional solar tracker. To do so, outdoor testing was conducted against a fixed-tilt control panel of identical make and model to the panel on the tracker. The methodology and results of this test can be found in Section 6.4.

6.1 Desired Angle Consistency Testing. Because the tracker moves at different speeds depending on whether it is expanding or contracting, two sets of testing were conducted to ensure that the tracker could reach any desired angle consistently. The first set of tests involved expanding the tracker from its fully contracted position to a specific angle, while the second set involved contracting the tracker from its fully expanded position to a specific angle. Both tests were conducted 10 times each for many different angles.

This test can be reproduced exactly by running the pytest file in the github repository linked here. The procedure is as follows:

- A Samsung Note 20 was mounted flat on the panel to measure the angle of the panel. The phone was calibrated to the ground before the testing procedure. The phone was running an app called "phyphox"[22] which uses the phone's accelerometer to plot the angle of the phone as a function of time in intervals of 1 second.
- The function `test_contraction_consistency()` tests the consistency of the desired angle by going repeatedly from the homed position at max_expansion_angle to every angle in Table 6(*a*) using the actuation time listed in the table for the respective angle. The position of each angle is held for 5 seconds to allow the mechanism to settle. The number of test repetitions is 10.
- The function `test_expansion_consistency()` tests the consistency of the desired angle by going repeatedly from the homed position at max_compression_angle to every angle in Table 6(*b*) using the actuation time listed in the table for the respective angle. Similar to the above function, the number of test repetitions is 10 and processing pauses for 5 seconds after each actuation. In this function, however, the actuator is first contracted to max_contraction before being expanded to the desired angle.

The angle vs time data for the contraction test is shown in Figure 17. This data is processed by extracting the final angle for each actuation time and plotting it against the actuation time as shown in Figure 18. From this plot it is clear that the tracker can achieve any desired angle from the homed position extremely consistently. Both the vertical and horizontal error bars which represent the standard deviation of the final angle measurements, and the standard deviation of the actuation time measurements respectively, are scaled by 10 to make them visible. The unscaled standard deviation of the final angle measurements is shown in Figure 19 with a peak of 0.55° at 19°. The residuals of the average final angle for each actuation time from the desired angle are shown in Figure 20. The residuals are smallest at 0 actuation time, indicating that the homing mechanism is very accurate. The residuals increase with actuation time, reaching a peak of around 1.5 degrees at 8 seconds of actuation time. This is acceptable for our purposes, as the power output of the solar panel is not significantly affected by a 1.5 degree error in the panel's angle.

The expansion test is necessary to ensure that the tracker can accurately reach any desired angle from its most fully contracted position. This position is furthest from the homed position and will therefore have the most error. The angle vs time data for the expansion test is shown in Figure 21. This data is processed by extracting the final angle for each actuation time and plotting it against the actuation time as shown in Figure 22. From this plot it is clear that the tracker can achieve any desired angle from the fully contracted position extremely consistently. Once again, both the vertical and horizontal error bars are scaled by 10 to make them visible. Although the standard deviation of the final angle measurements is larger than in the contraction test, it is still acceptable. The unscaled standard deviation of the final angle measurements is shown in Figure 23 with a peak of 0.65° also at

19°. The plot is much more uniformly scattered due to the lack of a homed starting position. The residuals of the average final angle for each actuation time from the desired angle are shown in Figure 24. The residuals are also roughly consistent throughout the test, with a peak of around 1.2 degrees at 4 seconds of actuation time. This is surprisingly less than the residuals during the contraction test, indicating that it is likely the lookup table from Table 21 that needs to be adjusted to improve accuracy.

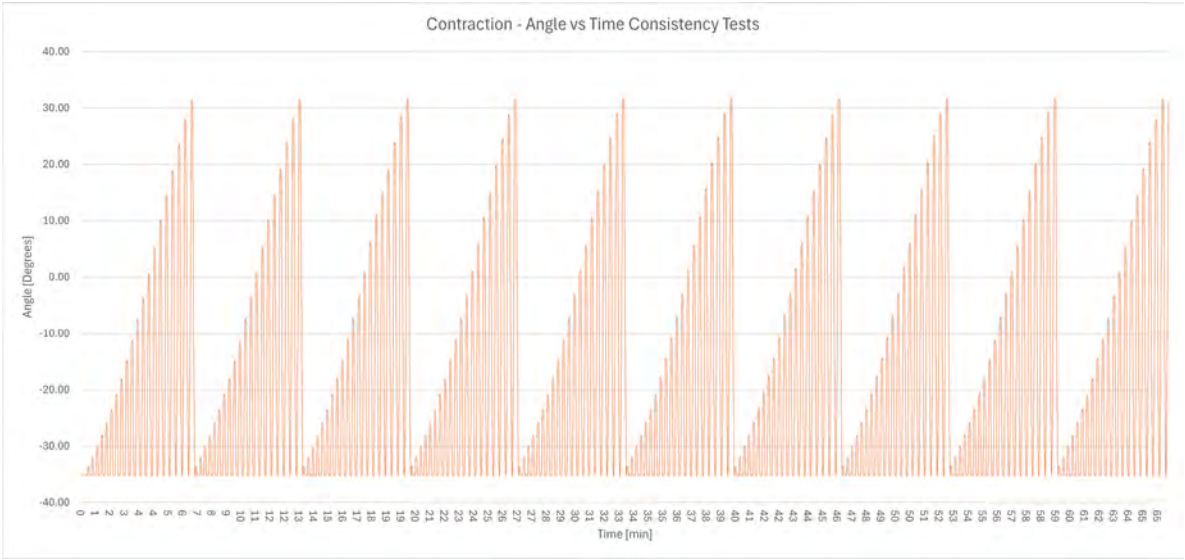

Fig. 17 Consistency Test for Tracking Angle from Full Expansion to a Specific Angle: The solar tracker is initially set to its maximum expansion at -35.2°. It is then adjusted to a particular angle by powering the actuator for the amount of time specified in Table 6(*a*) for that particular angle. This process is repeated for each angle listed in Table 6(*a*). To ensure consistency, this entire test is conducted 10 times, resulting in 10 data points for each angle.

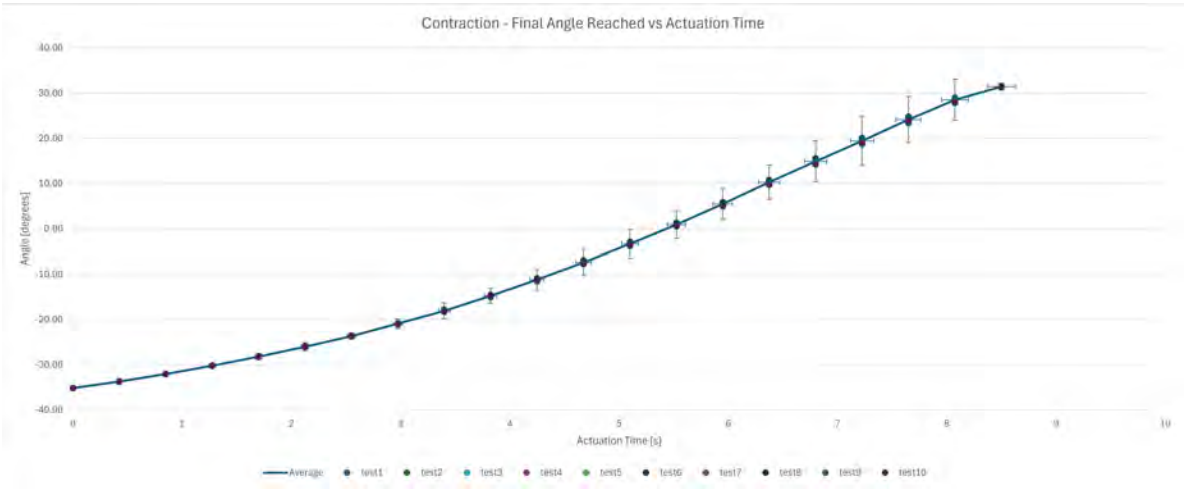

Fig. 18 Processed Data from Consistency Test: This graph shows the solar tracker's final angle versus actuation time. Horizontal error bars indicate the timing error associated with the accuracy of the Raspberry Pi's internal clock (10x standard deviation), this increases with actuation time. Vertical error bars show the standard deviation of final angle measurements (10x). Vertical error is only slightly larger than horizontal error, indicating that actuation time is the primary source of error.

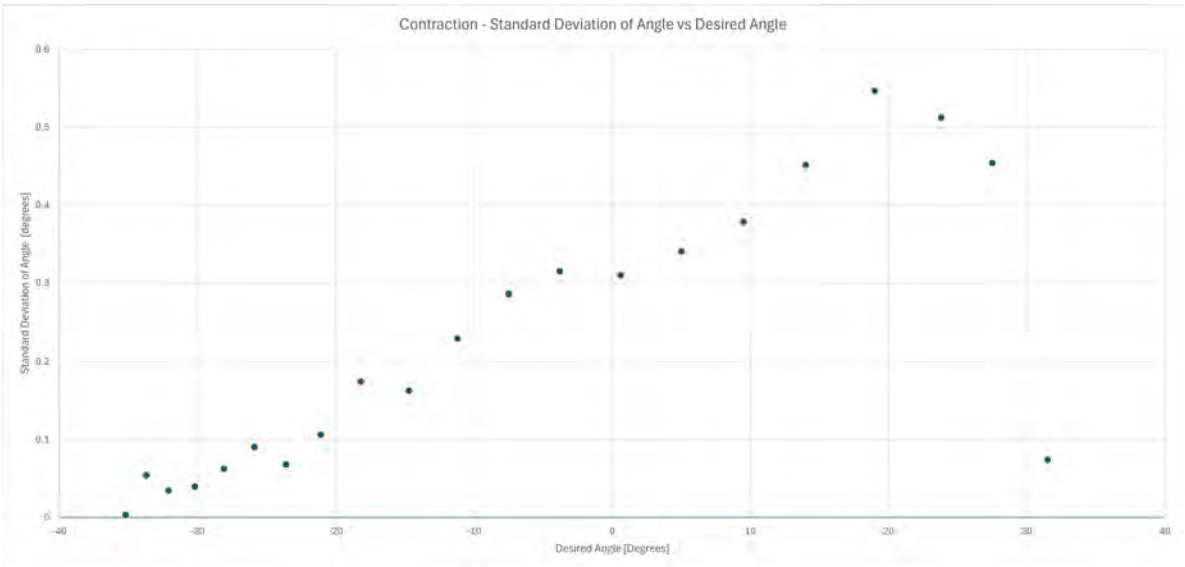

Fig. 19 Standard Deviation of Tracking Angle Measurements: The standard deviation of the final angle measurements is calculated for each actuation time. The standard deviation is smallest near 0 actuation time due to the homing mechanism ensuring near perfect alignment. The standard deviation increases with actuation time due to the Raspberry Pi's timing inaccuracy.

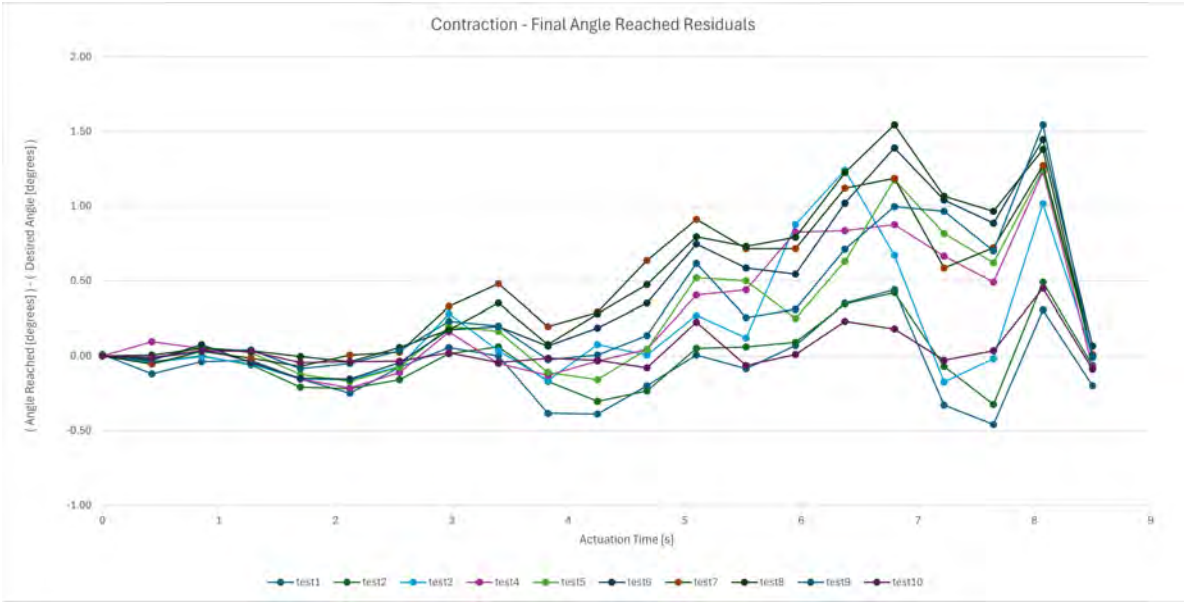

Fig. 20 Tracking Angle Consistency Test Residuals: The residuals are calculated by subtracting the average final angle for each actuation time from the actual final angle for each trial. This plot show residuals (on the y-axis) against actuation time (on the x-axis). Residuals are smallest near 0 actuation time due to the homing mechanism ensuring near perfect alignment. This indicates that error is unlikely caused by wobble in the mechanism and is instead due to the Raspberry Pi's timing inaccuracy. The remaining error is possibly due to inconsistent actuator speed, but further testing is required.

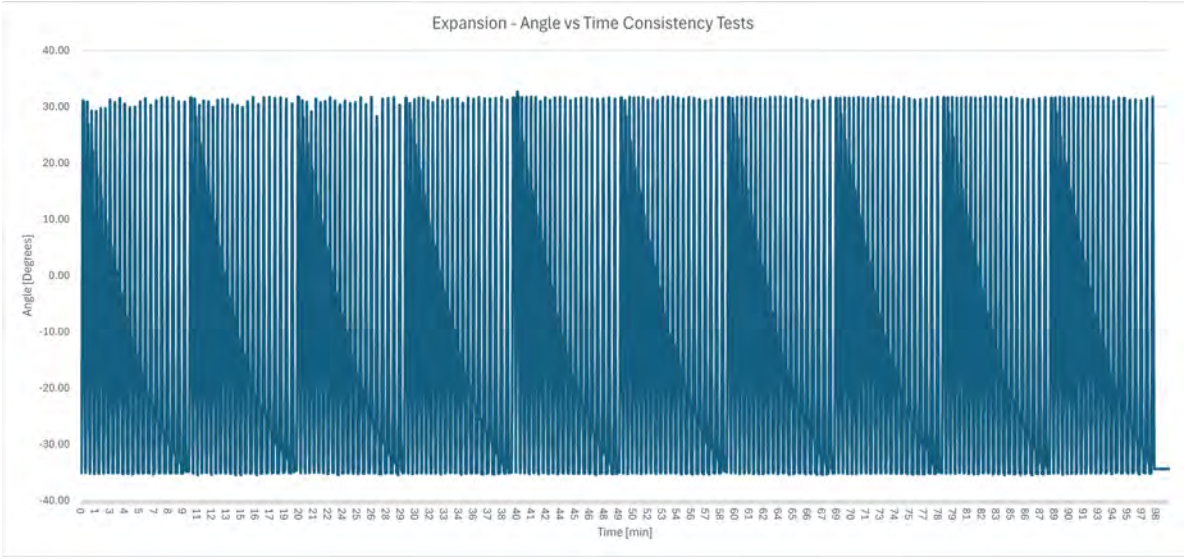

Fig. 21 Consistency Test for Tracking Angle from Full Contraction to a Specific Angle: The solar tracker is initially set to its maximum contraction at 31.5°. It is then adjusted to a particular angle by powering the actuator for the amount of time specified in Table 6(*b*) for that particular angle. The tracker is then homed to full expanion at -35.2° to avoid accumulating error. This process is repeated for each angle listed in Table 6(*b*). To ensure consistency, this entire test is conducted 10 times, resulting in 10 data points for each angle.

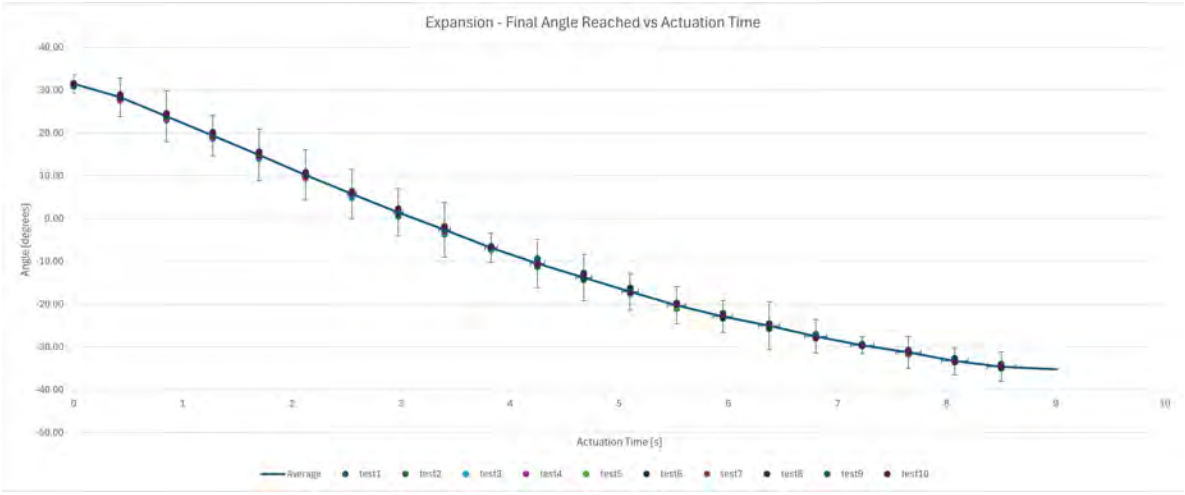

Fig. 22 Processed Data from Consistency Test: This graph shows the solar tracker's final angle versus actuation time. Horizontal error bars indicate the timing error (10x standard deviation) associated with the Raspberry Pi's internal clock, which increases with actuation time. Vertical error bars show the standard deviation of final angle measurements (10x). Vertical error is roughly consistent throughout the test because the tracker is set to its maximum contraction before each test instead of to a homed position like in the contraction test.

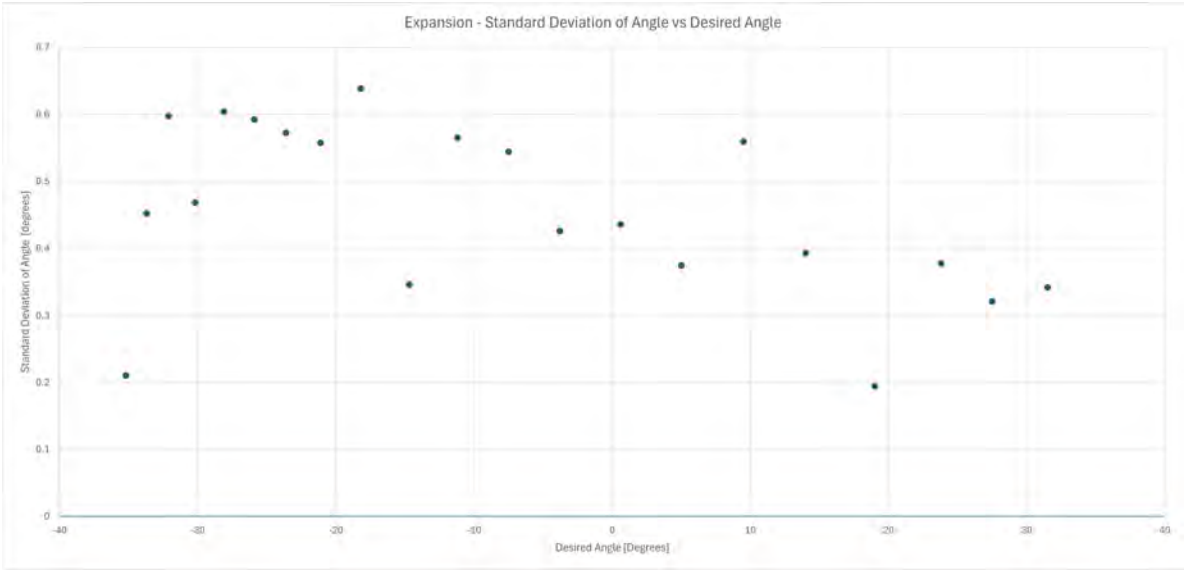

Fig. 23 Standard Deviation of Tracking Angle Measurements: The standard deviation of the final angle measurements is calculated for each actuation time. The standard deviation is evenly scattered throughout the test because the tracker is set to its maximum contraction before each test instead of to a homed position like in the contraction test.

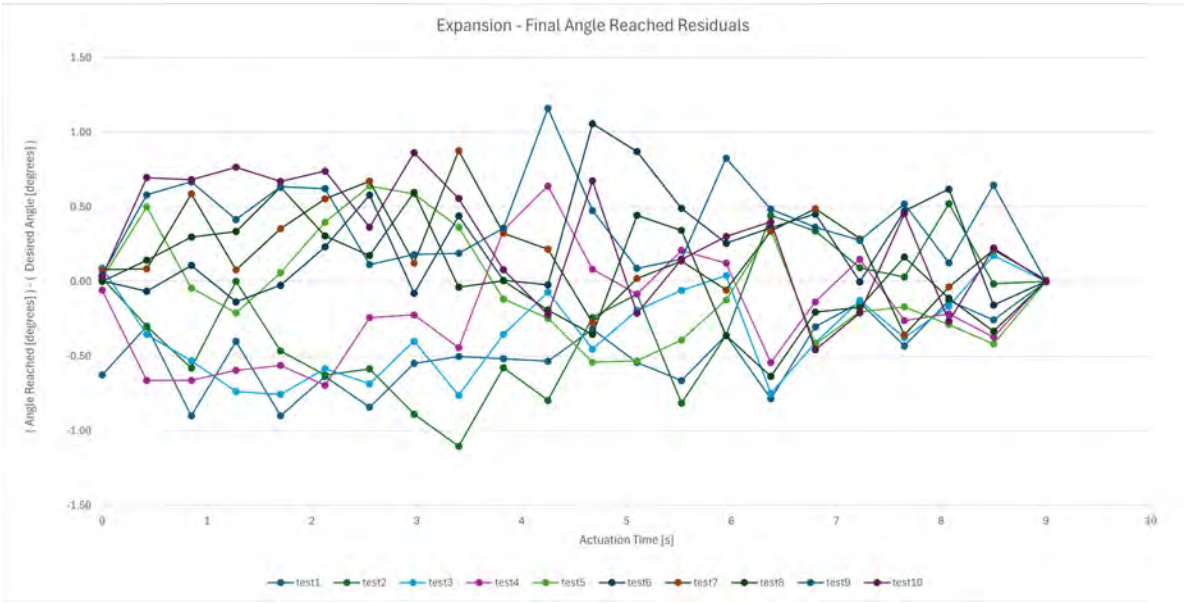

Fig. 24 Tracking Angle Consistency Test Residuals: The residuals are calculated by subtracting the average final angle for each actuation time from the actual final angle for each trial. Plots show residuals (on the y-axis) against actuation time (on the x-axis). Residuals are roughly consistent throughout the test because the tracker is set to its maximum contraction before each test instead of to a homed position like in the contraction test.

6.2 Fatigue Testing. To validate that the structure is robust and capable of withstanding the forces exerted on it during operation, a fatigue test was conducted. The test simply actuates the tracker from its fully contracted position to its fully expanded position and back again repeatedly. In the worst-case scenario, the tracker will do a full cycle from full compression to full actuation and back again every single day. To ensure all components of the mechanism can withstand this for the expected lifetime of the tracker, the test was conducted for 50 years worth of cycles. This is well beyond the 20 year life-expectancy of comparable solar trackers[4]. This test can be reproduced exactly by running the pytest file in the github repository linked here.

The function `test_fatigue()` tests the fatigue life of the tracker by actuating the tracker from its fully contracted position to its fully expanded position and back again repeatedly. The test is conducted for 50 years worth of cycles, which is roughly 18,250 cycles. The test concluded after 4 days without any noticeable wear. Additionally, the mechanism was also disassembled for inspection with no visible indication of permanent deformation or damage. This indicates that the tracker is robust and capable of withstanding the forces exerted on it during operation.

6.3 Input Power Usage Testing. Indoor power draw testing was conducted to validate that the input energy required to actuate the linear actuator and the additional energy required to overcome the stiffness of the flexures does not add up to significantly impact the net energy output of the tracker.

6.3.1 Test Setup and Procedure. For this test, we powered the linear actuator using a 12V power supply while using a voltmeter to measure the voltage drop across a Low-Ohm Resistor wired in series between the power supply and the linear actuator. The voltage drop and known resistance were then used to calculate the current through the loop, which was then used to compute the power input to the actuator. The instrumentation used for measuring the inclination angle was "phyphox" running on a Samsung Note 20, it is identical to the instrumentation used in Section 6.1. A diagram of the test setup is shown in Figure 25, where red represents power lines, yellow represents probe lines, and black represents the common ground. A 0.2 Ohm resistor was used because it is of low enough resistance to prevent excessive power from being dissipated while still being large enough to measure a reliable voltage drop. An oscilloscope was used to measure voltage over time since it is extremely accurate and supports the exporting of data to a computer.

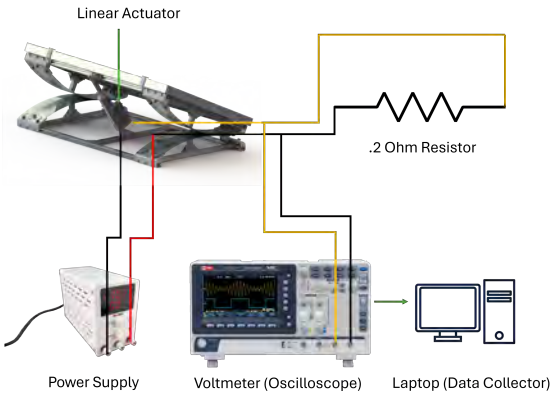

Fig. 25 Setup for Input Power Testing

6.3.2 Test Results. Two tests were performed: a compression test where the panel is swept from the fully expanded position of the actuator to the fully compressed position and an expansion test where the panel is swept from the fully compressed position of the actuator to the fully expanded position. The sign convention for our tracker angles is shown in Figure 26

(*a*) Fully Expanded Position

(*b*) Fully Compressed Position

Fig. 26 Angle Sign Convention

Our tests produced time series results for power and angle, which we then combined to create power-angle and energy-angle results. Integration of the power-time result was used to obtain energy results.

Figure 27 and Figure 28 represent the instantaneous power draw at each angle during the compression and expansion tests, respectively. Figure 29 and Figure 30 represent cumulative energy input as the panel is swept through its full range of motion during the compression and expansion tests, respectively. The energy-angle plots exhibit a strong fit for a linear relationship, with R^2 values of around 0.999. This means that while the work input differs depending on whether the actuator is compressing or expanding, the work input required for a given change in angular displacement during compression is constant regardless of what angle we start from. The same applies during expansion.

This is also expressed in Table 7, which reports the (constant) slopes of the energy-angle curves in Figure 29 and Figure 30. These results show that expansion moves through any given angle take approximately 1.8 times as much energy as compression moves through the same angle.

Lastly, if we add up the cumulative energy inputs from the expansion and compression tests, we get approximately $20J + 35J = 55J$. This number is referenced later in Section 6.4 when analyzing the total output energy during our outdoor test.

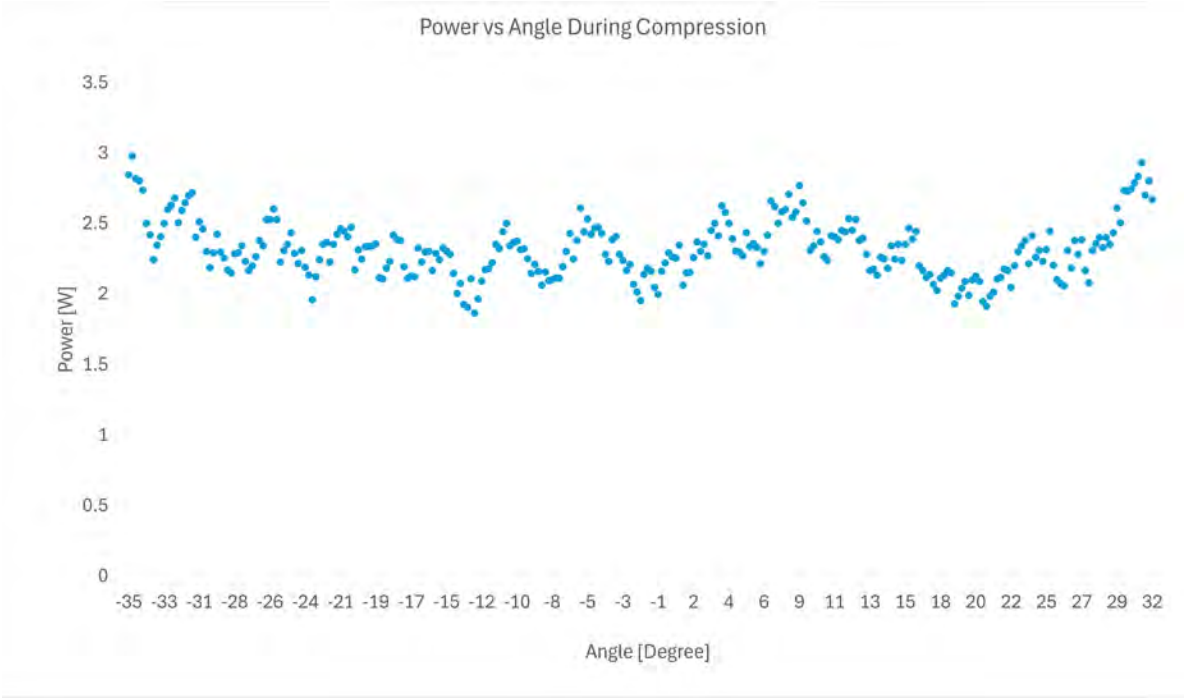

Fig. 27 Power Draw During Compression Test: The calculated power draw of the linear actuator is plotted against the angle of the solar panel during the compression test from full expansion at -35.2° to full compression at 31.5°

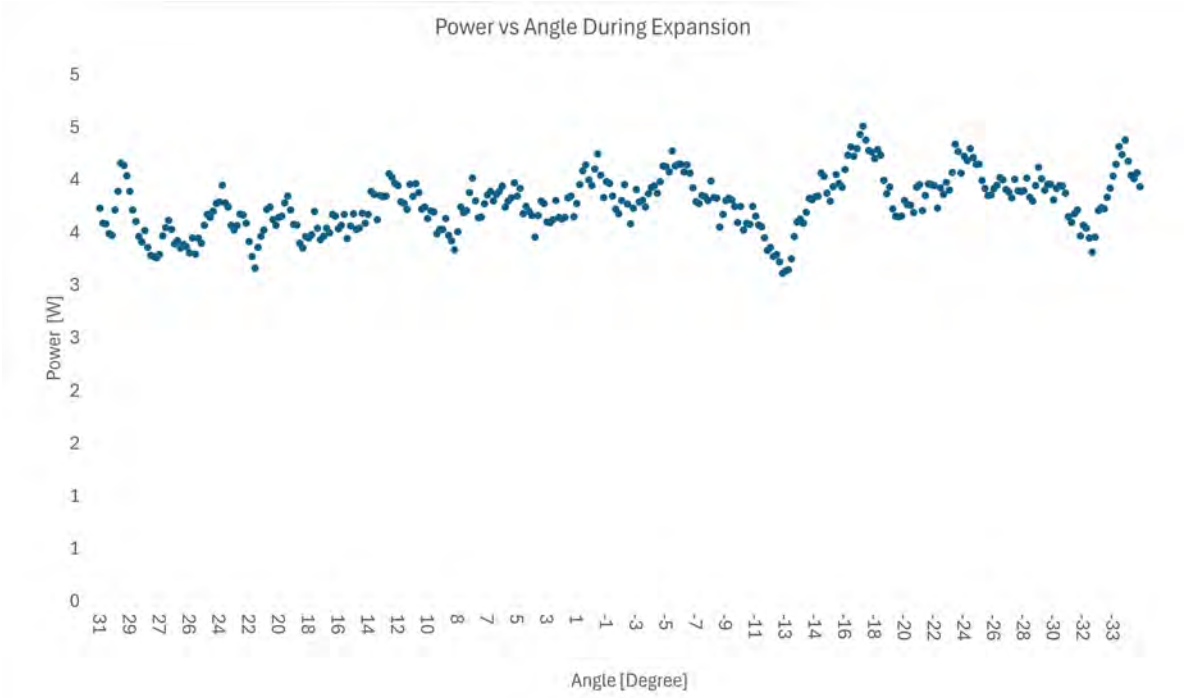

Fig. 28 Power Draw During Expansion Test: The calculated power draw of the linear actuator is plotted against the angle of the solar panel during the expansion test from full compression at 31.5° to full expansion at -35.2°

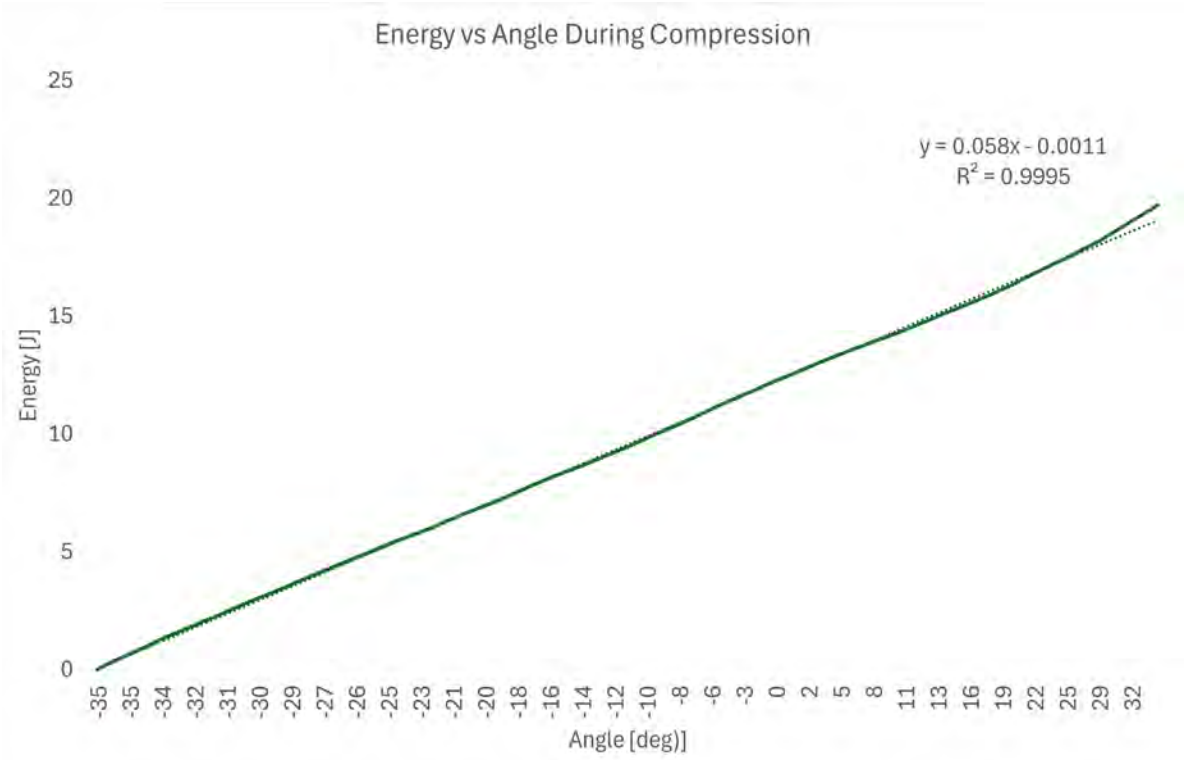

Fig. 29 Energy Usage During Compression Test: The calculated energy usage of the linear actuator is plotted against the angle of the solar panel during the compression test from full expansion at -35.2° to full compression at 31.5°. The dotted line is a line of best fit defined by the equation shown in the figure.

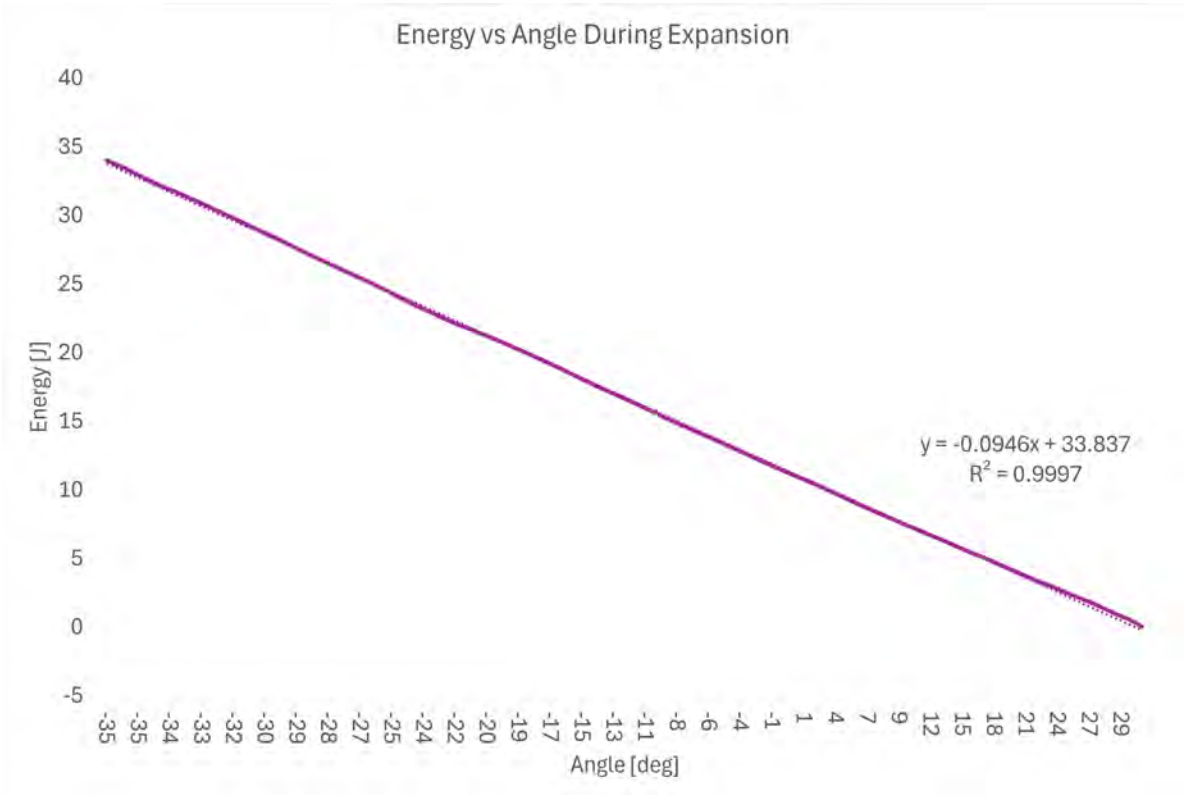

Fig. 30 Energy Usage During Expansion Test: The calculated energy usage of the linear actuator is plotted against the angle of the solar panel during the expansions test from full compression at 31.5° to full expansion at -35.2°. The dotted line is a line of best fit defined by the equation shown in the figure.

Table 7 Energy Usage During Motion

Angle Change Direction	Energy Usage per Angle Change [J/deg]
Compresssion	0.29
Expansion	0.52

6.4 Outdoor Output Power Testing. To validate the performance of our solar tracker, we conducted outdoor testing against a fixed-tilt control panel of identical make and model to the panel on the tracker. The test was conducted from sunrise to sunset on 5/4/2024, on a flat rooftop in Brooklyn, NY with shading only in the North direction (shading in this direction has the least impact on solar irradiance). Unfortunately, this day was very cloudy, averaging 90% cloud coverage.

6.4.1 Test Setup and Procedure. Due to the nature of this test depending on weather and solar irradiance, it unfortunately cannot be reproduced exactly. However, similar results can be achieved by running the code in the github repository linked here. The procedure is as follows:

- A Motorola Moto G4 is mounted flat on the panel to measure the angle with respect to the ground. The phone is calibrated to the ground before the testing procedure. The instrumentation setup for measuring inclination angle is identical to the setup used in Section 6.1 apart from the device used.
- A load resistor of 20 ohms is connected across the output wires of both the fixed panel and the tracking panel. A multimeter is connected in parallel to the load resistor to measure the voltage across the load resistor. The voltage is measured every 20 minutes and recorded. The power output of the panel is calculated by dividing the voltage by the resistance of the load resistor. The power output is then multiplied by the time interval to get the energy output in Wh.
- Running the script start_panel_process from the github repo starts the solar tracking process. The test is conducted over an entire day from sunrise to sunset. The update interval is set to 20 minutes, resulting in 46 movements throughout the day

6.4.2 Test Results. The angle measurements of the solar tracker during the test are shown in Figure 32. The total energy input to the solar tracker during the test is shown in Figure 33. The total power output of both the tracker panel and the fixed panel during the test is shown in Figure 34

Using the energy usage equations during compression that were calculated in Section 6.3 in conjunction with the angle measurements shown in Figure 32, the total energy usage over the course of the test day was calculated. As shown in Figure 33, the energy input for 5/4/2024 totals to 20J which corresponds to the energy usage during a full compression cycle. Referencing Table 8, the 20J total input energy accounts for only 0.001% of the total output energy of the tracker panel.

The results in Figure 34 show that the difference in output power between the fixed panel and the tracker panel is greatest in the hours directly succeeding sunrise and preceding sunset. This is because at those times, the Sun's elevation angle (angle up from the horizon) is relatively low, necessitating tilting in order to make incident rays normal to the panel surface. At mid-day, the sun is directly overhead, which is why the output power performance between the fixed and tracker panel are essentially identical.

To better characterize the tracking performance of our device, Table 8 tabulates results from our test alongside data from Kuttybay et al. [23] where two types of single-axis solar trackers (Light-Dependent-Resistor and Schedule based) along with a fixed-tilt

Fig. 31 Outdoor Testing Setup: This picture was taken the day before the actual test day. The tracker is in the homed position awaiting the command to start tracking.

control panel were tested in cloudy weather. In both experiments, the energy output of the tracking panel was compared to the energy output of the fixed panel to determine the average power increase obtained through solar tracking. For the *Total Energy Output*, our tracker put out a total of 372.1 Wh while the LDR and Schedule based trackers from [23] respectively put out 357 Wh and 372 Wh.

The *Normalized Energy Output* was calculated as

$$\frac{\text{Energy Output}}{\text{Panel Wattage}}$$

This is important because the panel used in [23] was a 60W panel while our panel is a 100W panel. Notably, if the two experiments are comparative, the *Normalized Energy Output* for the fixed panels should be around the same since their output is purely dependent on environmental factors and panel quality. Since the *Normalized Energy Output* for the fixed panel in [23] is much larger than our fixed panel's *Normalized Energy Output*, we use the ratio between the two as a scaling factor to calculate the *Normalized Average Power Increase*. This quantity can be thought of as the power increase we would see if our experiment was conducted under the same conditions as the experiment in [23].

Taking this into account, the *Normalized Average Power Increase* for our tracker was 29.71% while the LDR and Schedule based trackers from [23] respectively achieved 32.30% and 37.70%.

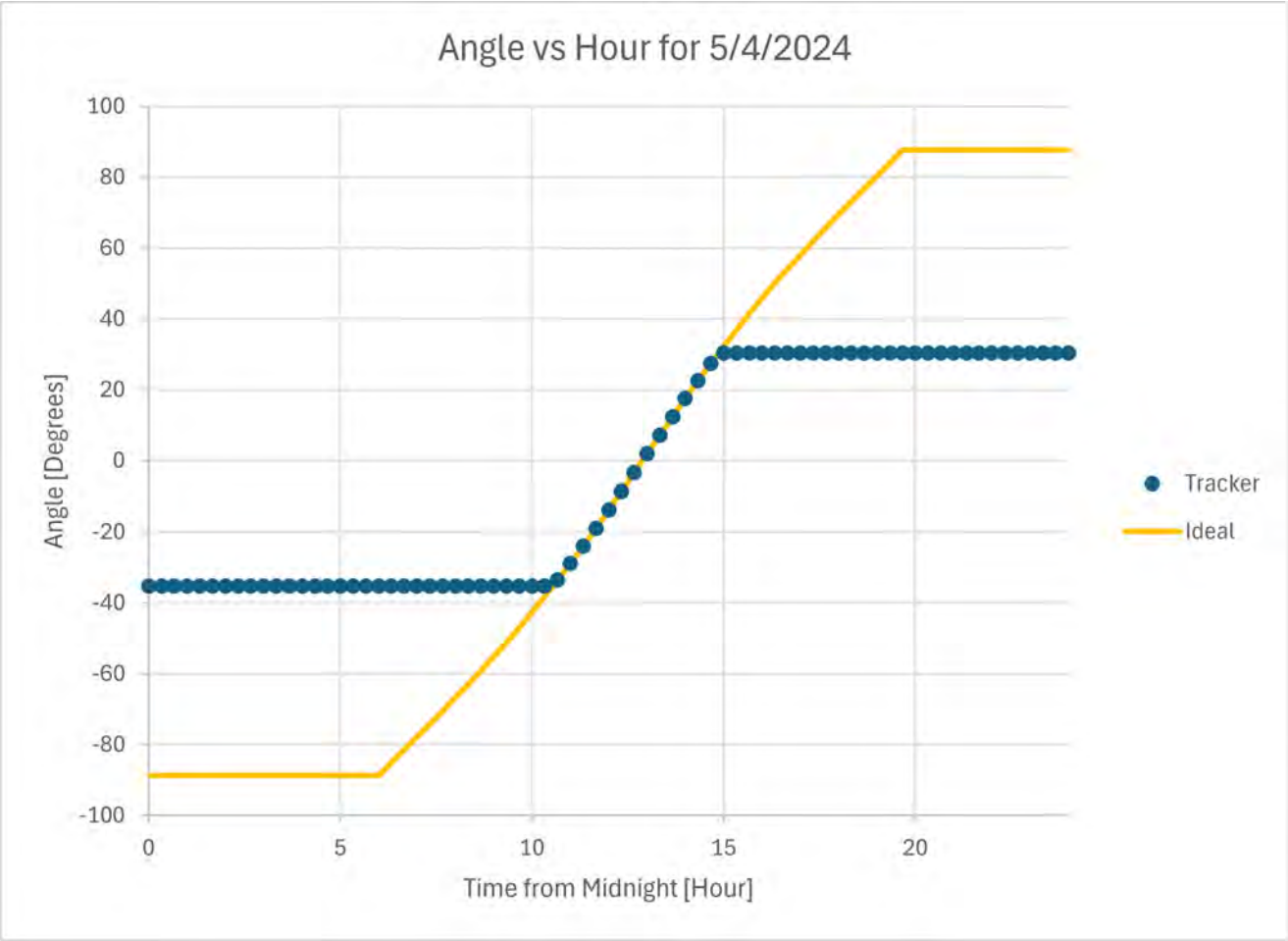

Fig. 32 Angle Measurements of the Solar Tracker During Outdoor Testing vs Time: The ideal case assumes an infinite range of motion of the solar tracker and a perfectly unobstructed horizon. The solar tracker updates every 20 minutes resulting in 46 movements throughout the day.

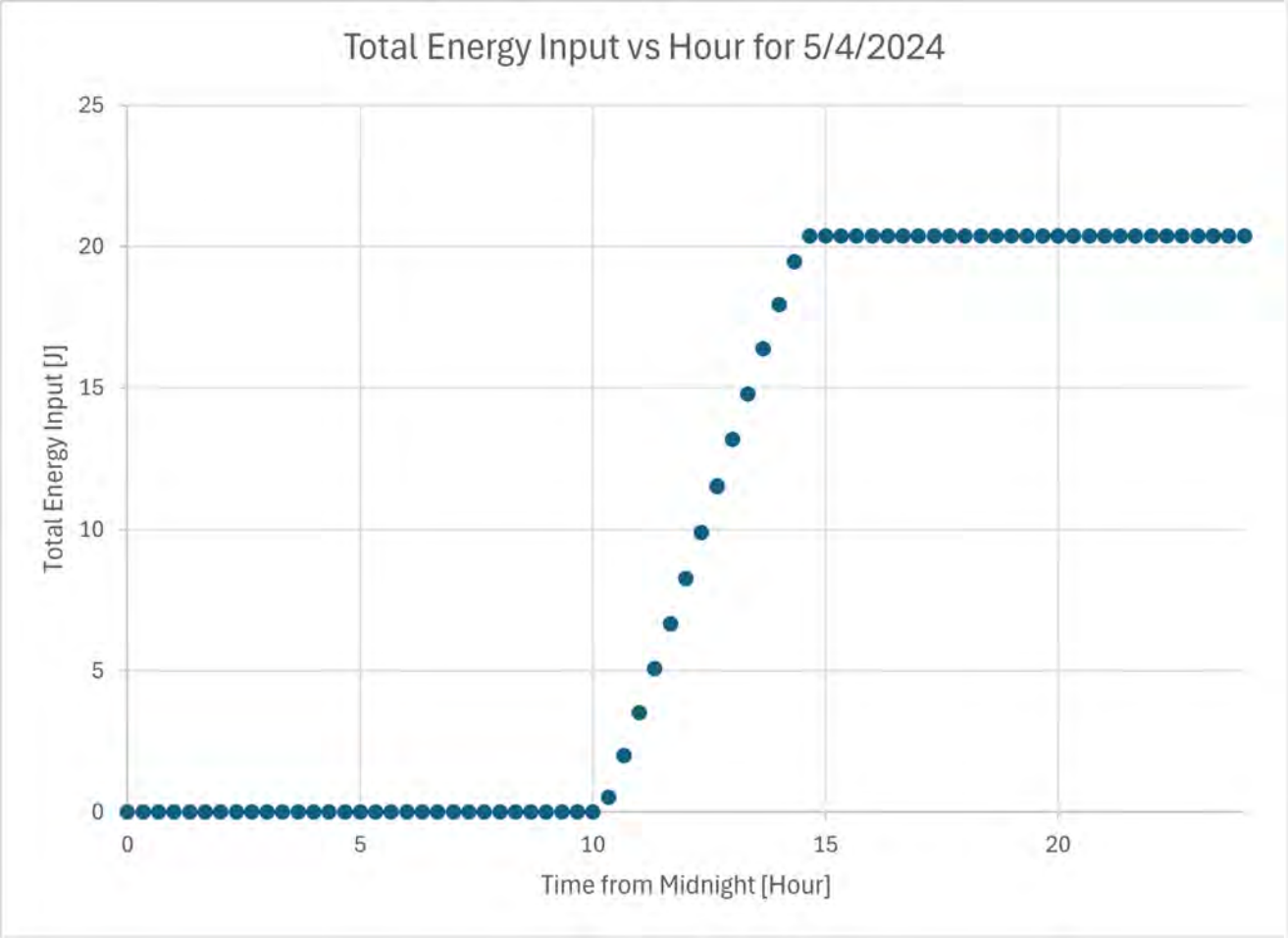

Fig. 33 Predicted Total Energy Input of the Actuator During Outdoor Testing vs Time: The equations for input energy vs angle change in Section 6.3 were used in conjunction with the angle measurements from the outdoor testing data to calculate the input energy required for each movement of the actuator. These were then sequentially summed to achieve the total input energy for each time during the test.

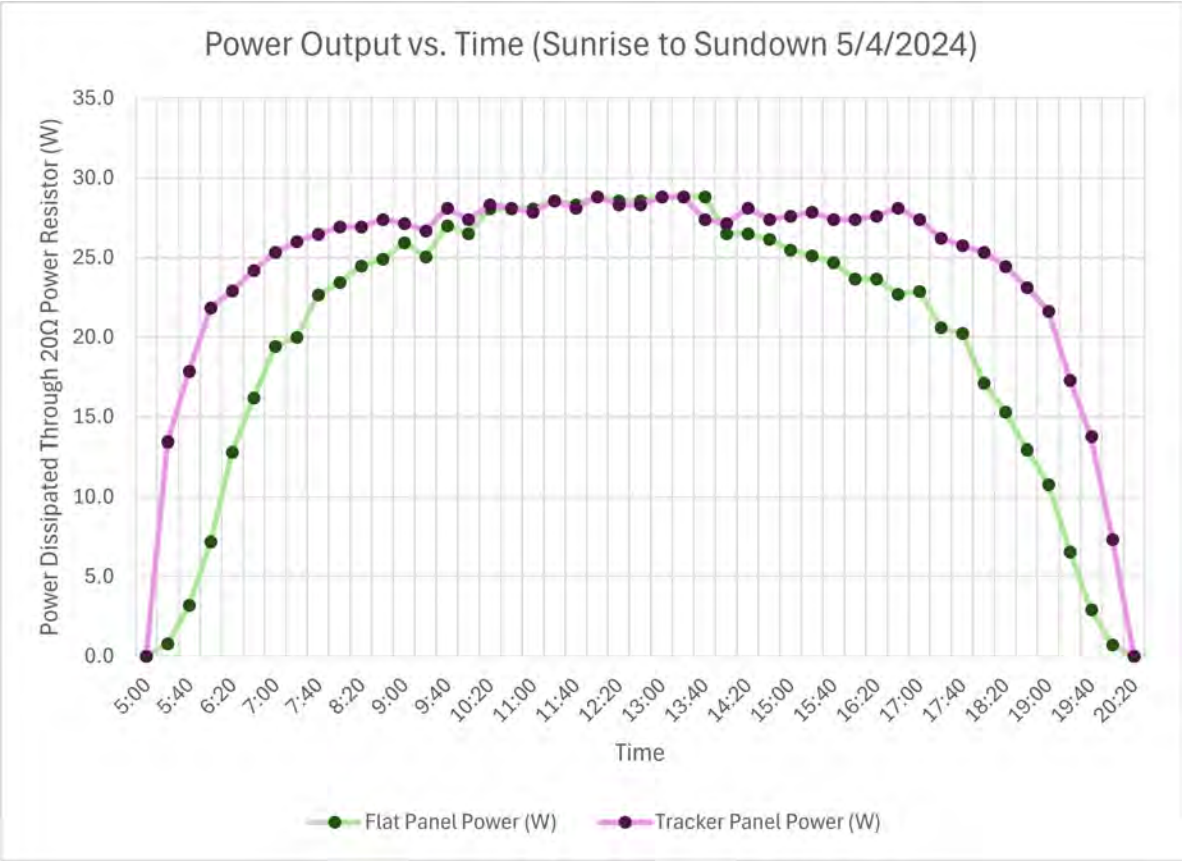

Fig. 34 Power Output of the Solar Panel vs Time During Outdoor Testing: The pink line represents the power output of the panel on our compliant solar tracker. The green line represents the power output of an identical fixed panel placed nearby. At noon, the power output is roughly equivalent because both panels are at the same angle, for all other times, the tracking panel outperforms the fixed panel as expected.

Table 8 Comparison of Our Experiment and Baseline Experiment

	Our Experiment		Baseline Experiment		
	Fixed Panel	Compliant Tracker	Fixed Panel	LDR Tracker	Schedule Tracker
Average Power Dissipation (W)	20.2	24.3	NA	NA	NA
Total Energy Output (Wh)	309.0	372.1	270	357	372
Normalized Energy Output (Wh/W)	3.09	3.72	4.50	5.95	6.2
Normalized Average Power Increase	Ref. Value	29.71%	Ref. Value	32.20%	37.70%

7 Final Remarks

This section aims to evaluate the final design against the cost and performance criteria established in Section 3.1. While certain aspects, like the panel's durability in extreme weather conditions, were not thoroughly tested, all other specifications have been met exceptionally well.

7.1 Cost Requirement. The initial cost requirement for the solar tracker was less than 5 times price of the panel it mounts. The cost breakdown for all the components is shown in Table 9. The cost after production is calculated using bulk pricing for 1000 units from [24] and [25]. Our prototype mounts a 100 W panel which can be purchased (without bulk pricing) for around $50. Because we are comparing to the cost of the solar panel after seller markup, it make sense to scale our final production cost by a typical selling markup. With a final production cost of $75, our tracker is less than 1.5 times the cost of the panel it mounts without accounting for markup. After applying a typical 50% imposed markup, our design could be purchased for $113. This is still only 2.3 times the cost of the panel it mounts. Even without mass production, our design still meets the cost requirement at 4.4 times the price of the panel.

Table 9 Cost Breakdown for Single Unit vs Production (Estimated for 1000 Units)

Item	Purchase Cost	Production Cost
Flexure Bands	$34.82	$15.61
Contact Rollers	$35.37	$17.22
Linear Actuator	$28.59	$10.00
Framing	$42.00	$24.28
Electronics	$56.89	$2.14
Mounting Hardware	$20.00	$5.40
Total Cost	$217.67	$74.65

Compared to other rooftop solar trackers, our design appears to be significantly less expensive. The least expensive rooftop trackers we can find such as rocking solar, and the PV Booster, sell for $350, and $800 respectively. Although it is difficult to tell how much they are marking up the price of their products, our design is significantly cheaper than both of these options. Even without mass production and a 50% markup, our design would sell for $330 which is still cheaper than all existing alternatives.

Although we did not test the tracker outside over the course of a year, it is reasonable to assume from our fatigue testing that the tracker would require maintenance much less frequently than the current standard of twice a year. The linear actuator has an expected lifespan of 10 years and there are no gears or bearings to lubricate which is normally the main source of solar tracker maintenance. We expect our tracker to operate maintenance free for several years.

Using the national average cost of electricity of 0.18 USD/kWh[26], the amount of time it would take to offset the cost of our system at its marked up selling cost of $113 is less than 1 year as shown in Equation 2.

$$\text{Payback Period} = \frac{\$113}{\left(\frac{\$0.18}{\text{kWh}}\right) \times (100\text{W})} \tag{1}$$

$$\text{Payback Period} = 0.72 \text{ Years} \tag{2}$$

This offset period would be greater with the cost of installation, although the ease of assembly of our design ensures that this additional cost is comparable to other rooftop tracking alternatives.

7.2 Performance Requirement. The initial performance requirement for the solar tracker was to achieve a 30% increase in gross energy output compared to a fixed-tilt system. As shown in Section 6.3, our solar tracker uses around 55J of energy to complete a full expansion and full compression cycle. Section 6.4 demonstrates that even on the cloudy day that the system was tested on, the tracking panel output an additional 118J of energy compared to the fixed panel which results in a 29.7% increase in gross energy output. On a sunny day, this performance is expected to be significantly higher.

8 Future Work

During the assembly and testing phase of our design, several areas of improvement were discovered. In addition, there is a large variety of testing that can be performed to further validate our design.

8.1 Mechanical Design. As mentioned earlier, although we designed the tracker to achieve 40 degrees compression and expansion, after assembly it only achieves a compression angle of 31.5 degrees and an expansion angle of -35.2 degrees. By decreasing the radius of the contact rollers, the line tangent with the contact roller at the fully compressed and expanded positions will be steeper, allowing the panel to reach a greater angle. This will however require a decent amount of redesign and testing.

While the small 70 mm extrusions in the middle of each contact roller provides rigidity, it also increases the cost and complexity of the assembly. By increasing the thickness of the sheet metal used for the contact rollers, it may be possible to remove this component entirely without sacrificing too much rigidity. The cost benefit analysis of this should be explored.

While we mounted a 100 W panel on our solar tracker, a larger 150 W panel could be mounted instead without any major modifications. Mounting a panel larger than a 150 W panel is still feasible but would require the tracker dimensions to be scaled horizontally so that the edge of the panel does not touch the ground at full compression and expansion. This could potentially further increase the cost efficiency and payback period for the system.

8.2 Software Design. Although the current state of the code includes a function that pulls weather and solar irradiance data from the internet to optimize the path and update interval of the tracker, this function is not yet implemented. This function would be a great addition to the code as it would allow the tracker to only actuate when it will result in a net increase in power output. This would be especially useful on cloudy days, where updating the position of the tracker fewer times throughout the day would result in a net increase in power output.

The current code also does nothing about excessive wind. If the wind is strong enough, it could potentially damage the tracker. A function that pulls wind data from the internet and moves the tracker to an optimal position to minimize wind resistance would be a great addition to the code.

8.3 Testing. No testing was done on the tracker's ability to withstand wind or other loads such as snow. This is a critical area of testing that needs to be done before the tracker can be used in a real-world application. The tracker should be tested in a wind tunnel to ensure that it can withstand high wind speeds.

Although fatigue testing was performed, it is yet to be seen how the mechanism will resist the elements over time. The structure is made of 6061 aluminum which is unlikely to rust, however, the speed of the actuator might be affected by excessive cold or heat. If this is indeed the case, an accelerometer or encoder would need to be implemented instead of the time based algorithm currently employed.

Acknowledgment

We would like to express our gratitude to our advisor, Professor Michelle Rosen, for her invaluable guidance, unwavering support, and insightful suggestions throughout this project.

Appendix A: Technical Drawing of Mounting Plate

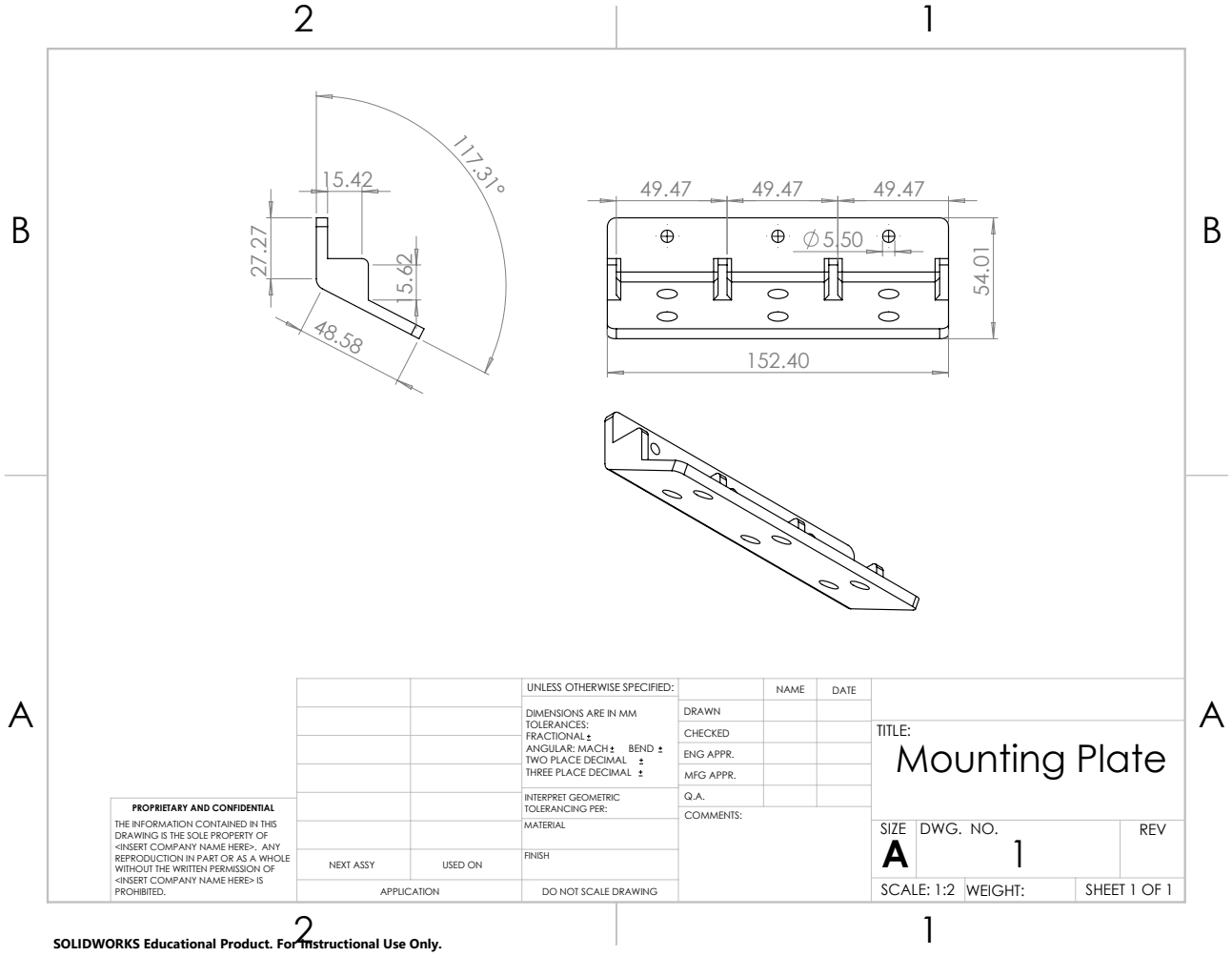

Appendix B: Technical Drawing of Contact Roller

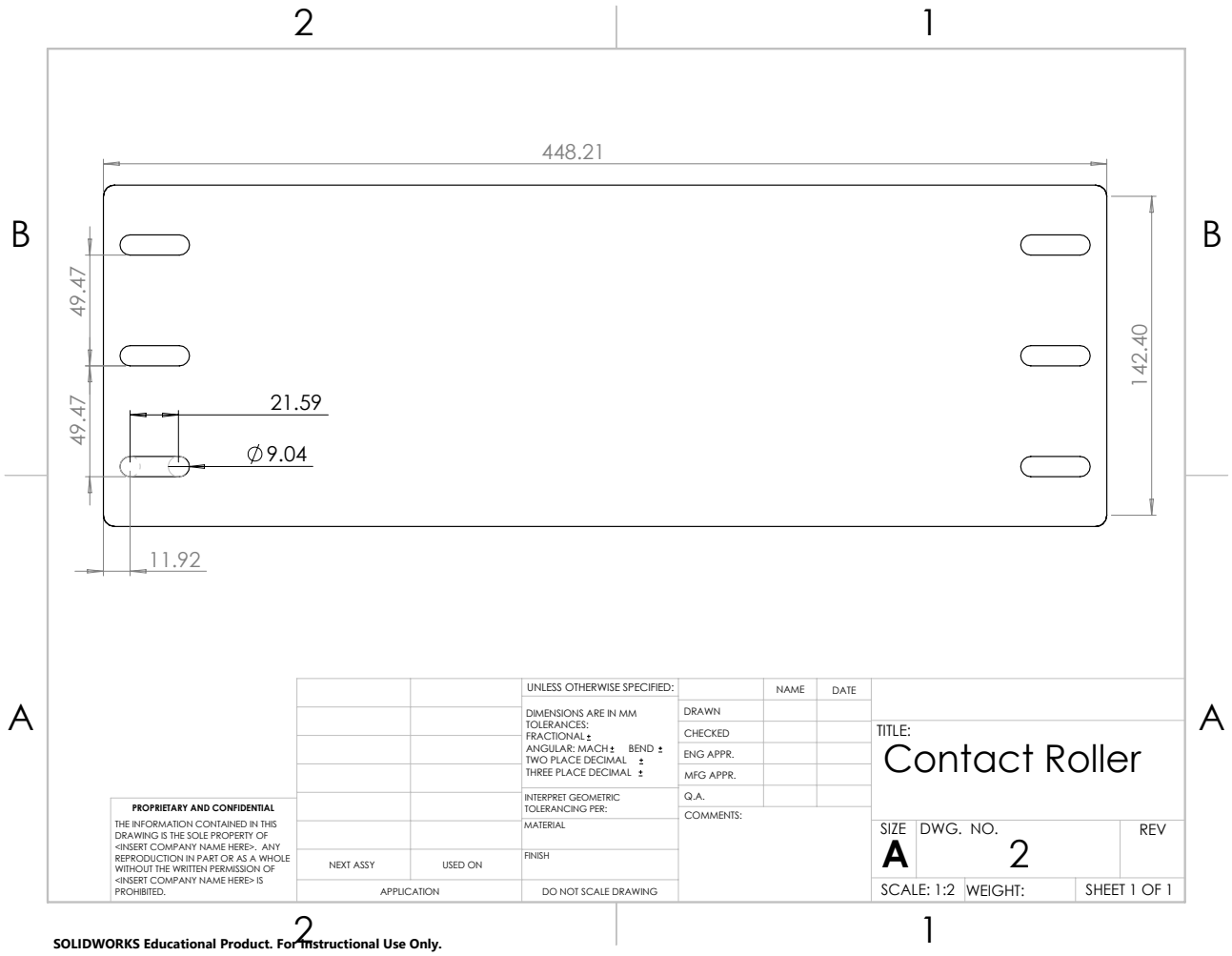

Appendix C: Technical Drawing of Flexure

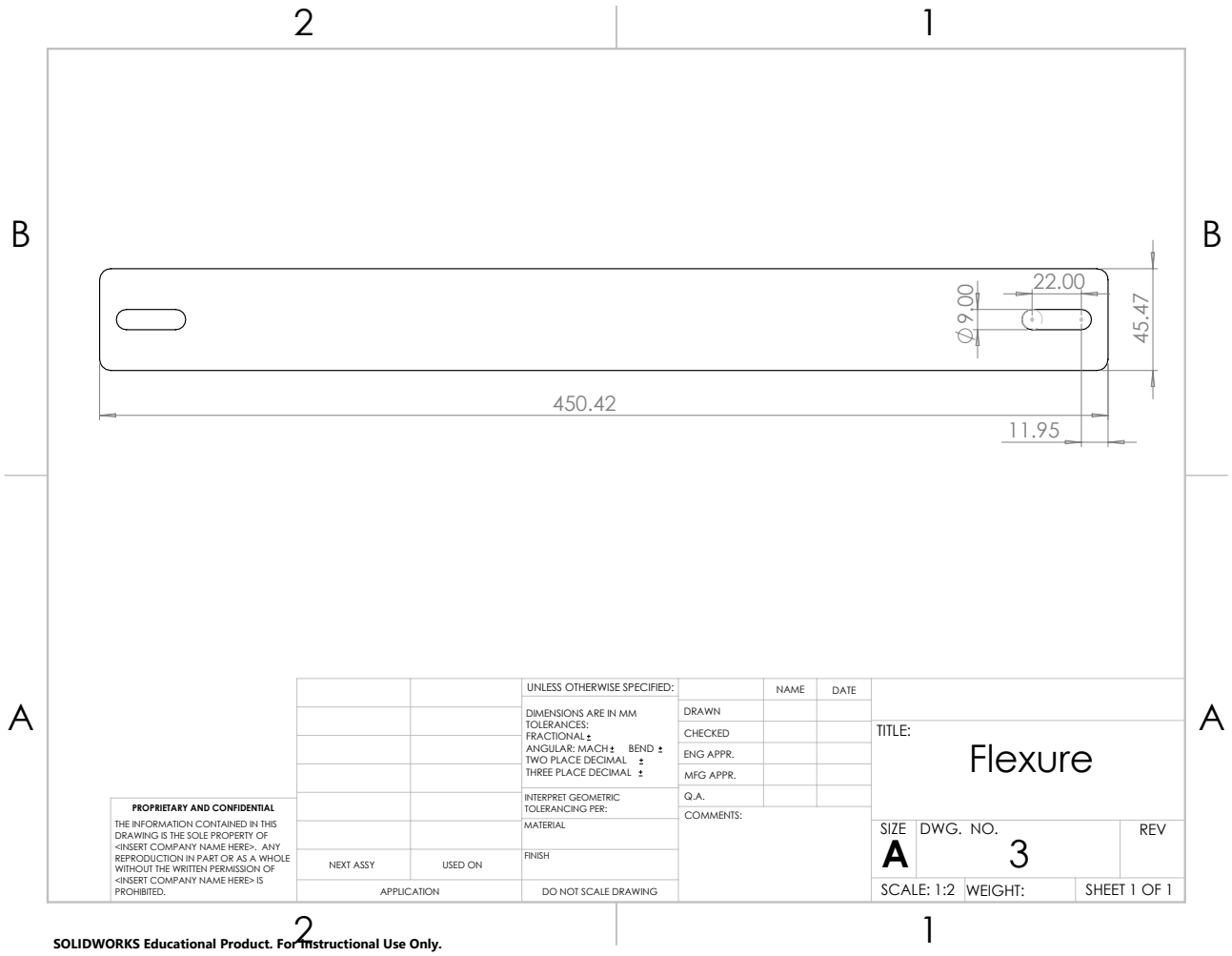

Appendix D: Technical Drawing of Panel Bracket

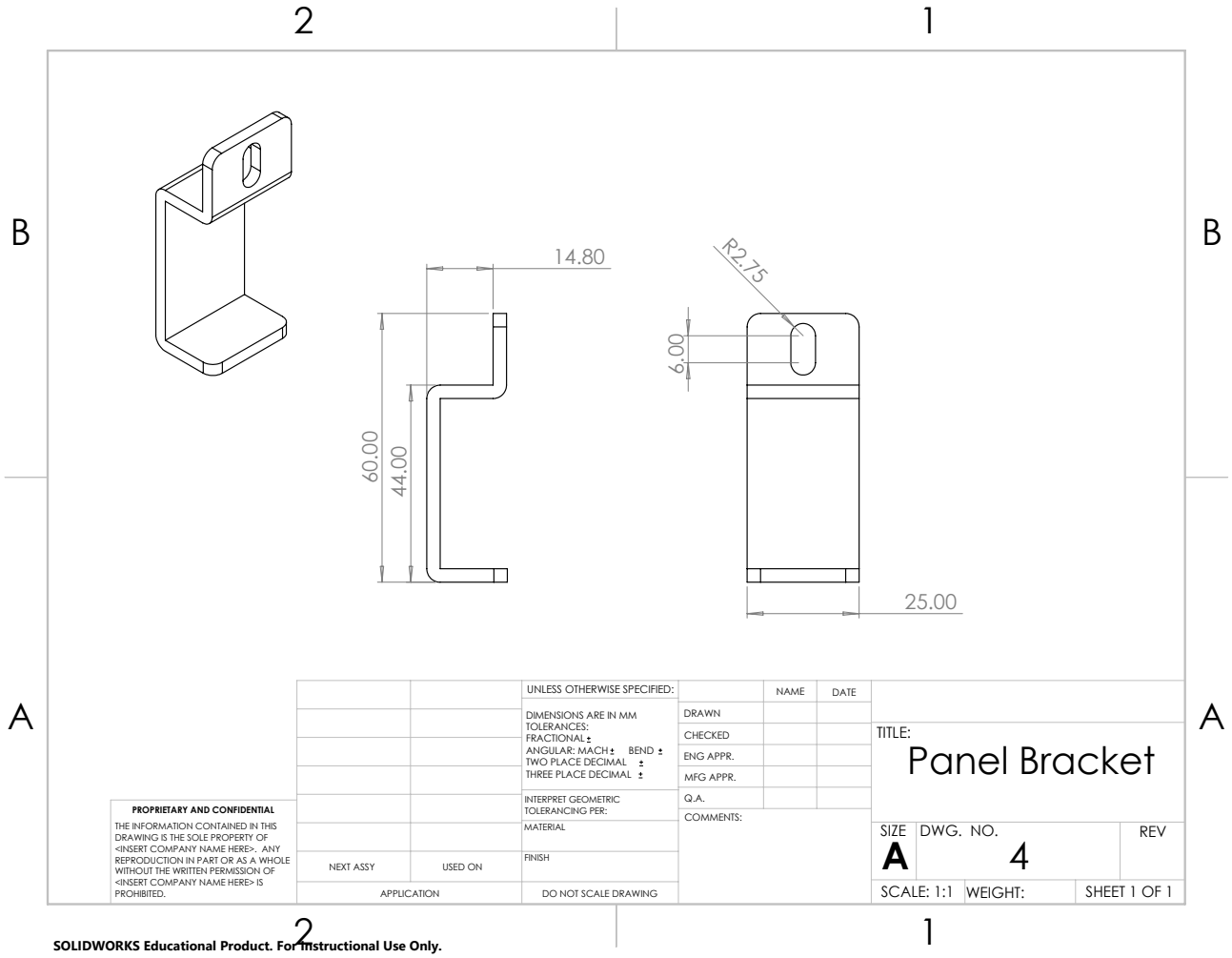

Appendix E: Technical Drawing of Top Actuator Bracket

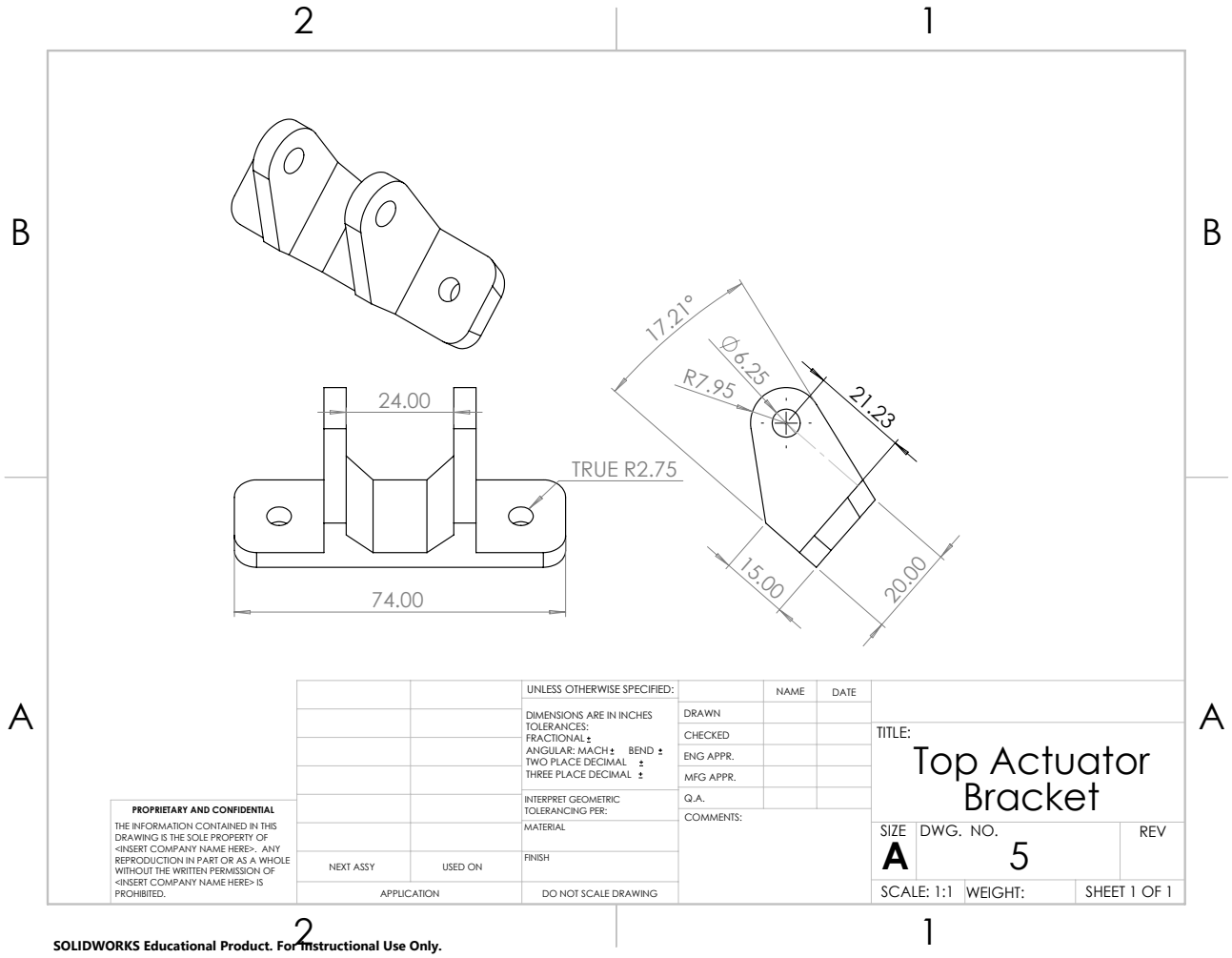

Appendix F: Technical Drawing of Bottom Actuator Bracket

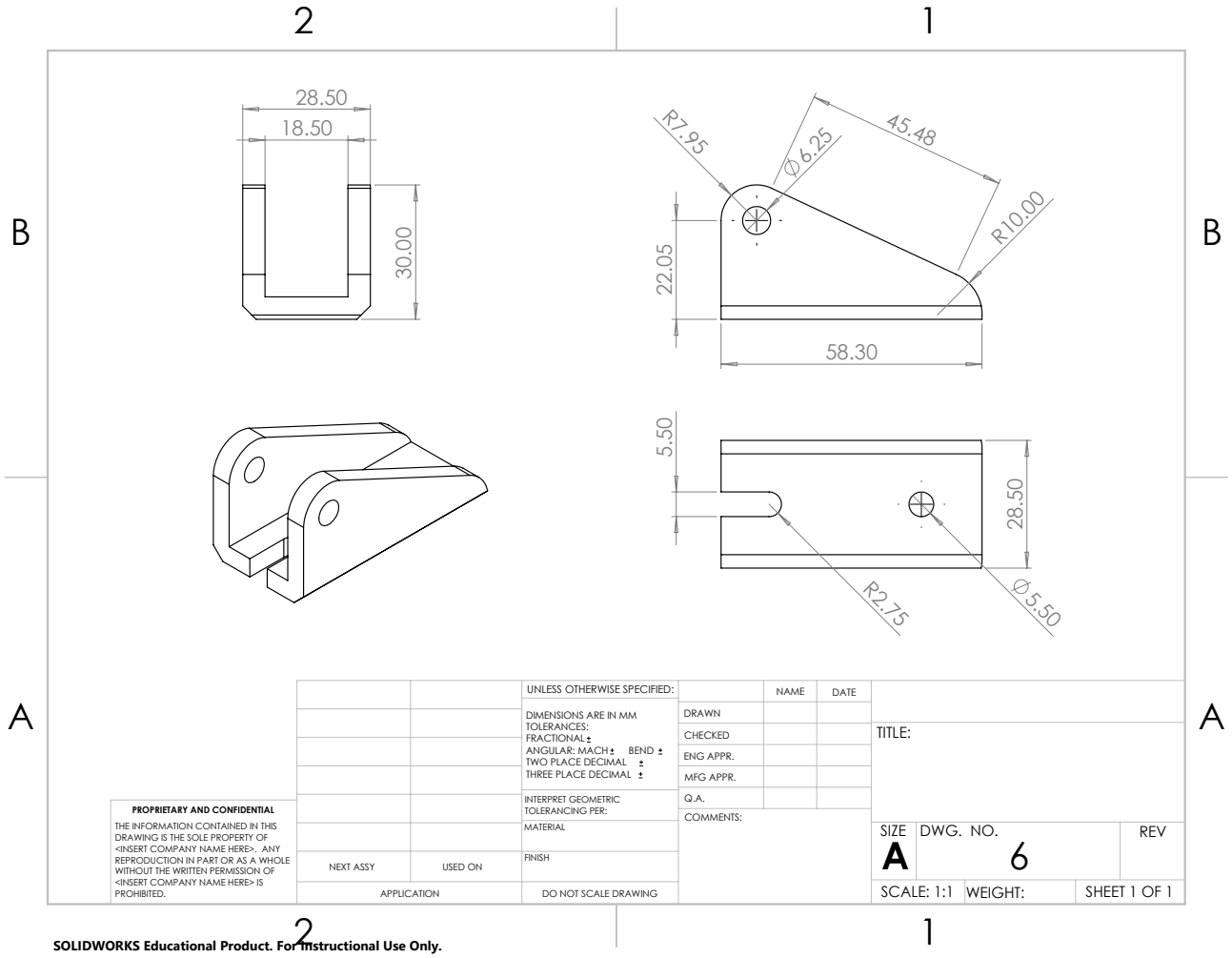

References

[1] U.S. Energy Information Administration, Year of Access, "More than 50% of the United States has Favorable Solar Resources," https://www.eia.gov/todayinenergy/detail.php?id=30912#:~:text=More%20than%2050%25%20of%20the,solar%20resources%20are%20more%20favorable.

[2] Logan, P. E. and Raichle, B. W., 2017, "Performance Comparison of Fixed, Single, and Dual Axis Tracking Systems for Small Photovoltaic Systems with Measured Direct Beam Fraction," ASES National Solar Conference.

[3] 2016, "Advantages and Disadvantages of Solar Tracker System," Solar Power World.

[4] Bahrami, A., Okoye, C. O., and Atikol, U., 2017, "Technical and economic assessment of fixed, single and dual-axis tracking PV panels in low latitude countries," Renewable Energy, **113**, pp. 563–579.

[5] Agyekum, E., Afornu, B., and Ansah, M., 2020, "Effect of Solar Tracking on the Economic Viability of a Large-Scale PV Power Plant," Environmental and Climate Technologies, **24**, pp. 55–65.

[6] RevPart, 2024, "Living Hinge Design: The Ultimate Guide," https://revpart.com/living-hinge-design-guide/.

[7] Evke, E., Huang, C., Wu, Y.-W., Arwashan, M., Lee, B., Forrest, S., and Shtein, M., 2020, "Kirigami-Based Compliant Mechanism for Multiaxis Optical Tracking and Energy-Harvesting Applications," Advanced Engineering Materials, **23**, p. 2001079.

[8] Howell, L. L. and Midha, A., 1980, "Compliant mechanisms," Journal of Mechanical Design, **124**(2), pp. 223–235.

[9] Trees, . B., 2023, "Solar Panel Sun Tracker: Better Solar Panel Angle For Extra Cost?" https://8billiontrees.com/solar-panels/solar-panel-sun-tracker/

[10] Musa, A., Alozie, E., Suleiman, S. A., Ojo, J. A., and Imoize, A. L., 2023, "A Review of Time-Based Solar Photovoltaic Tracking System," Information, **14**(4).

[11] International Code Council, 2018, *International Building Code*, 2018th ed., International Code Council, section 15.

[12] International Organization for Standardization, 2021, "ISO 14001: Environmental management systems - Requirements with guidance for use," ISO, Geneva, Switzerland, Standard ISO 14001:2021.

[13] International Electrotechnical Commission, 2017, "IEC 61724-1:2017: Photovoltaic system performance monitoring - Part 1: Guidelines for measurement, data exchange and analysis," IEC, Geneva, Switzerland, Standard IEC 61724-1:2017.

[14] Linß, S., Henning, S., and Zentner, L., 2019, "Modeling and Design of Flexure Hinge-Based Compliant Mechanisms," *Kinematics*, J. Mizrahi, ed., IntechOpen, Rijeka, Chap. 3.

[15] Shaw, L. A., Chizari, S., Dotson, M., Song, Y., and Hopkins, J. B., 2018, "Compliant rolling-contact architected materials for shape reconfigurability," Nature Communications, **9**(1), p. 4594.

[16] EnergySage, 2023, "100-Watt Solar Panels: Are They Enough For You?" https://www.energysage.com/solar/solar-panel-output/100-watt-solar-panels-are-they-right-for-you/.

[17] Troiano, E., 1986, "Evaluation of Corrosion Resistant Surfaces on 6061 Aluminum Alloy," .

[18] Espressif Systems, 2021, *ESP32-C3-WROOM-02 Datasheet*, https://www.espressif.com/sites/default/files/documentation/esp32-c3-wroom-02_datasheet_en.pdf

[19] Anderson, K., Hansen, C., Holmgren, W., Jensen, A., Mikofski, M., and Driesse, A., 2023, "pvlib python: 2023 project update," Journal of Open Source Software, **8**(92), p. 5994.

[20] Anderson, K. and Mikofski, M., 2020, "Slope-Aware Backtracking for Single-Axis Trackers," National Renewable Energy Laboratory, https://www.nrel.gov/docs/fy20osti/76626.pdf

[21] Yahr, G. T., 1997, "Fatigue design curves for 6061-T6 aluminum," Journal of Pressure Vessel Technology-transactions of The Asme, **119**, pp. 211–215.

[22] Staacks, S., Hütz, S., Heinke, H., and Stampfer, C., 2018, "Advanced tools for smartphone-based experiments: phyphox," Physics Education, **53**(4), p. 045009.

[23] Kuttybay, N., Saymbetov, A., Mekhilef, S., Nurgaliyev, M., Tukymbekov, D., Dosymbetova, G., Meiirkhanov, A., and Svanbayev, Y., 2020, "Optimized Single-Axis Schedule Solar Tracker in Different Weather Conditions," Energies, **13**(19).

[24] "Digi-Key Electronics," Website, https://www.digikey.com/

[25] "McMaster University," Website, https://library.mcmaster.ca/citing-sources

[26] New York State Energy Research and Development Authority, 2024, "Monthly Average Retail Price of Electricity," https://www.nyserda.ny.gov, Last updated: April 11, 2024.